Scientific report WR 96-02

KNMI

Chaos and Coupling: A coupled atmosphere ocean-boxmodel for coupled behaviour studies

G. Zondervan

In cooperation with Utrecht University, Department of mathematics

De Bilt, 1996

Scientific report= wetenschappelijk rapport; WR 96-02

De Bilt, 1996

Postbus 201
NL-3730 AE De Bilt

Telephone +31.30.220 69 11, telefax +31.30.221 04 07

UDC: 551.526.63
551.465.5
51
ISSN: 0169-1651
ISBN: 90-369-2106-6

Chaos and Coupling

A coupled atmosphere ocean-boxmodel for coupled behaviour studies

G. Zondervan

KNMI, De Bilt, The Netherlands

March 26, 1996

I would like to thank dr. Theo Opsteegh and prof. Ferdinand Verhulst for their intelligent suggestions and interesting remarks during my research. Their differing approaches to my problem proved to be very inspiring. Furthermore I would like to thank everybody else in the Predictability group for their interest, enthousiasm and help along the way, and providing me with the programs that I needed. Finally I would like to thank my girlfriend Hester for her support and patience.

Contents

1 Introduction

In this report the behaviour of a very simple coupled atmosphere/ocean system was investigated. The system consists of a chaotic atmosphere (the Lorenz '84 atmosphere model) coupled to a relatively slow ocean capable of having two stable regimes (after Stommel's two-box ocean model). Lots of numerical experiments are done with complex ocean and atmosphere models and a lot of effort is put in trying to parameterize natural processes in order to couple them realistically. Little is known however, about the effect coupling has on chaotic dynamical systems. Thus it seems useful to try to study the effect of coupling on a very simple chaotic system without trying too much to comply quantitatively with observed processes in reality. Several questions can be raised :

- Can certain techniques be constructed so as to efficiently find the 'new' attractor of the coupled system?
- Does the coupling to a slow ocean result in a correspondingly slow signal in the atmospheric variables?
- Does coupling to the ocean introduce essentially new dynamics?

It is especially the first question that was raised within the climate predictability group at KNMI, because with more complex coupled models the amount of computer-time is a serious limit on the analysis. And the transient to the attractor can be a lengthy process. In addition the basic phenomena may be obscured by many other effects. The subject of a chaotic system coupled to other systems is not very well investigated. The work presented here cannot give answers to the above raised questions. It can however give some new insight in the specific system that is examined, and some of the results may be aplicable to other coupled ocean-atmosphere or similar systems. The main question that is asked in this report is: "Can we measure an effect on the atmosphere if it is coupled to an ocean model that is driven entirely by this atmosphere?".

2 The Models

In this section we shall discuss what models have been used, and what motivation formed the basis of their choice. The models will be described in more detail in the respective sub-sections. The region of interest does not so much cover physical processes as it does model behaviour at a fundamental level. Therefore the models are basically chosen for their relative simplicity and the atmosphere model also for its chaotic behaviour.

The Atmosphere model was constructed by Lorenz in 1984 (Lorenz 1984), it contains three variables (X,Y,Z) and can with appropriate parameters display chaotic behaviour. Some investigations on this atmosphere model have been conducted

by Anastassiades (Anastassiades 1995). He found a window in parameter space for which this model probably behaves chaotically, as well as a way to make the complex dynamics of the model more clearly visible. Lorenz's model was constructed as a means of demonstration rather than one with which to produce realistic atmospheric behaviour. As Lorenz stressed in the article in which he introduced the model, : "the model...cannot yield much quantitative information. It may serve principally in examining hypotheses and formulating new ones. ". He had constructed it in a somewhat ad hoc manner, and although there are ways to derive the Lorenz model, from "realistic" quasi-geostrophic equations (see Saltzman 1989), it is due to this truncation that it is uncertain what values the variables should be taking in reality. The Lorenz model deals with one basic large scale atmospheric process. Namely that of the interaction between the westerly current and large scale eddy-like structures on the northern hemisphere. Basically the westerly current is driven by the meridional temperature gradient. The eddies are perturbations on this homogeneous flow field. They are forced by the zonal ocean-continent temperature contrast, and by the instability of the westerly current. The eddies transport heat polewards, thereby reducing the meridional temperature contrast. And stabilizing the westerly current. The three variables in this model and what they represent are:

- X : the intensity of the symmetric globe-encircling westerly wind current (and also the poleward temperature gradient assumed to be in permanent equilibrium with it)
- Y : the cosine phase of a chain of large superposed eddies
- Z : the sine phase of a chain of large superposed eddies

According to the article of Lorenz, these eddies are to be identified with Rossby waves.

The ocean model is a slightly modified Stommel two-box model (Stommel 1961). This model was not made to represent any real ocean but it is the simplest model demonstrating the opposing forces of the thermo-haline circulation. The two-box model is made to represent the large scale convection processes in either the north atlantic or near the equator. It displays in itself rather simple dynamics, however for an appropriate set of parameters it has two stable regimes of flow. The thermohaline flow develops either poleward or equatorward, depending on the initial conditions (i.e. the deep water formation is either near the equator or in the polar area). For other parameter settings it has only one stable solution, the flow being either poleward or equatorward depending on the parameters. I will first give a brief description of the two-box model followed by a description of the atmospheric model.

2.1 The Ocean Model

We shall now discuss the simple ocean model that has been used. Consider two reservoirs, each containing an equal and constant volume of water which is perfectly mixed in each of the boxes. The two boxes are interconnected via a pipeline at the bottom of both boxes. In general the densitiy of the water between the boxes will differ. And thus there will be a pressure imbalance at the pipeline, and a flow will occur between the two boxes. The pipeline through which the water will flow has a certain flow-resistance k. And at the top there is an overflow so that the volume of water in each of the boxes is kept constant. So when a certain amount of water flows from one box to the other through the pipeline, the same amount flows back via the overflow. For a schematic drawing of the system see figure 1.

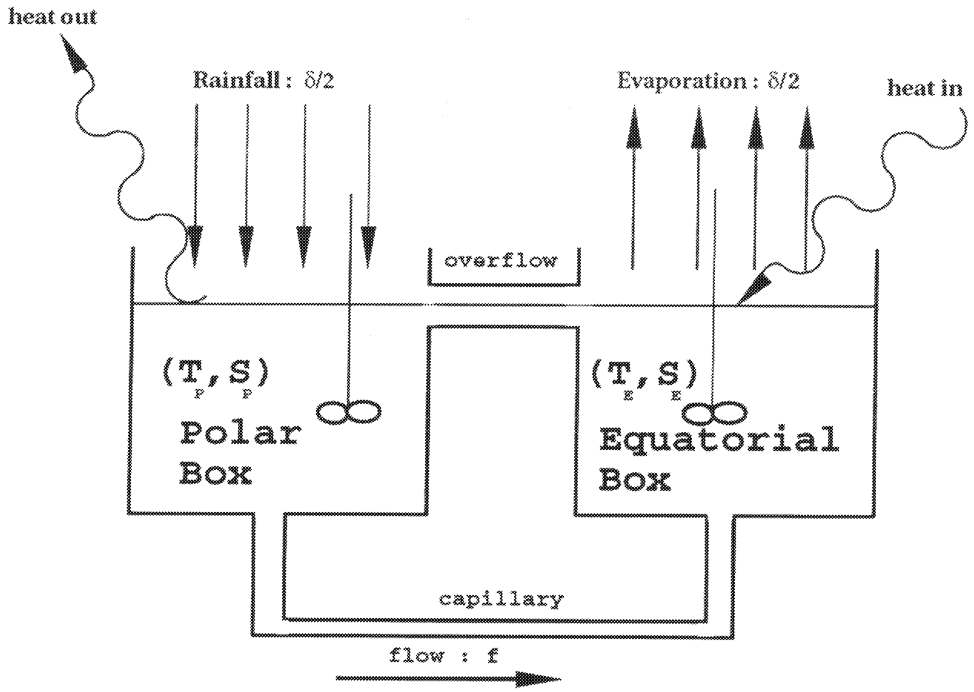

Figure 1: The Two-box model

The density of the water is supposed to be only dependent on its temperature (T) and salt content (S). And the relation is approximated by a linear relation :

$$\rho = \rho_0(1 - \alpha T + \beta S) \tag{1}$$

The size and direction of the flow f between the two boxes is linearly dependent on the density (pressure) difference between the boxes.

$$kf = \Delta\rho = \beta\Delta S - \alpha\Delta T \tag{2}$$

As can be seen from the above equation the strength and direction of the flow is governed by two opposing forces or density effects : a higher temperature reduces

the density of the water, and a higher salinity increases the water density. In our model one of the boxes is named the polar box and represents the northern-half of the ocean. This box is supplied with a quantity of 'fresh water' or, because in this model the volume is kept constant, with a negative salt flux. This flux represents precipitation in the polar areas. This is where we differ from Stommel's model (see below). The polar box is also coupled to the (cold) atmosphere and will lose heat linearly proportional to the temperature difference between the atmosphere and the ocean. The other box is named equatorial box and represents the equatorial area of our ocean model. This box loses water through evaporation, represented by a positive salt flux and gains heat. Depending on the relative strength of these external forcings the flow can develop either poleward when temperature driven or equatorward when driven by the salinity difference. The model differs from Stommel's, because whereas Stommel used as forcing a relaxation relation towards a prescribed salinity and temperature , we use a flux forcing for the salinity and only a relaxation relation for the temperature. This is done so that the coupling to the atmosphere can be conducted later on. The two equations describing the evolution of the ocean model are put here in terms of difference in temperature and salinity between the two boxes, since it is only the difference in these values between the boxes that drives the flow. Note that the exchange of properties of the water between the two boxes is insensitive to the direction of the flow, reflected here by the absolute value of the flow in the equations.

$$\dot{T} = k_a(T_{at} - T) - |f|T - k_w T \tag{3}$$
$$\dot{S} = \delta - |f|S - k_w S \tag{4}$$
$$f = \omega T - \xi S \tag{5}$$

Where T is the temperature difference between the polar and the equatorial box and S is the salinity difference between the two. And the parameters are :

k_a : the coefficient for heat exchange between the ocean and the atmosphere.

T_{at} : the temperature difference between the polar and equatorial air.

k_w : the internal diffusion of the ocean (through the overflow, between box boundaries).

δ : the equivalent salt-flux of the water transport (equals the precipitation at the pole plus the evaporation at the equator).

In this model no water is absorbed by the atmosphere so the evaporation equals the precipitation. The flow is determined by the last equation. The parameters ω and ξ combine the effects of the density dependence (of both salinity (via β) and

temperature (via α)) and the flow resistance in the pipeline, as follows : $\omega = \alpha/k$ and $\xi = \beta/k$. The flow is considered positive when in poleward direction. For an equilibrium solution holds : $\dot{T}_{eq} = \dot{S}_{eq} = 0$, this leads to :

$$T_{eq} = \frac{k_a T_{at}}{(k_a + |f_{eq}| + k_w)} \tag{6}$$

$$S_{eq} = \frac{\delta}{(|f_{eq}| + k_w)} \tag{7}$$

$$f_{eq} = \omega T_{eq} - \xi S_{eq} \tag{8}$$

Let Φ be defined as : $\Phi(f_{eq}) \equiv \omega T_{eq} - \xi S_{eq}$, with T_{eq} and S_{eq} given in equation (6-7). An equilibrium solution for the thermohaline flow can be written as :

$$\Phi(f) = f \tag{9}$$

A graphical solution of the above equations, see figure 2, gives us some insight in the possible equilibria. The displayed curve is Φ as a function of f. The intersection between the curve and the straight line indicates a possible solution, there are two curves in display each corresponding with a certain set of parameters. It can be shown that there is a range of parameters for which there exist two stable regimes of flow : a sluggish flow which is salinity driven and equatorward (this is the negative direction) and a faster temperature driven flow poleward. The final direction of the flow is then dependent on the initial state of the ocean. There is also an unstable solution consisting of a slow poleward flow, but since it is unstable it will not show up in computer simulations. For other sets of parameters there is either the salinity driven flow or the temperature driven flow (not displayed here).

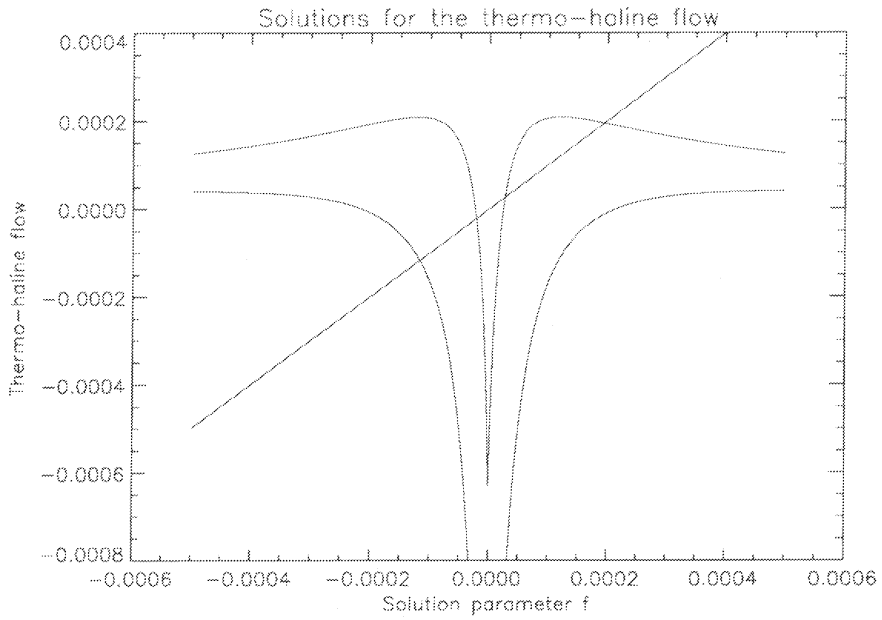

Figure 2: Solutions of the thermohaline flow (Φ) for two sets of parameters

2.2 The Atmosphere Model

The atmosphere model consists of the following three differential equations :

$$\dot{X} = -Y^2 - Z^2 - aX + aF \quad (10)$$
$$\dot{Y} = XY - bXZ - Y + G \quad (11)$$
$$\dot{Z} = bXY + XZ - Z \quad (12)$$

Where the dotted terms represent the derivatives with respect to time. The terms XY and XZ in equations (11) and (12) represent the gain of energy of the eddies, at the expense of the westerly current : the terms $-Y^2$ and $-Z^2$ in equation (10) (the eddies transport heat polewards and thereby reduce the north-south temperature anomaly). The variables have been scaled so that the coefficients for the damping of the waves are unity, thereby defining the timescale. Where one unit of time corresponds with five days. The eddies can also be displaced by the westerly current and this is represented in the terms $-bXZ$ and bXY. Note that if b is greater than unity the waves are displaced more than they amplify. The linear terms take care of damping processes, both mechanical and thermal; the damping time for the eddies has been chosen as the time unit. Again note that if a is less than unity the westerly current damps less rapidly than the eddies. The driving factors (or thermal forcing) for both westerly current and the eddies lie in the terms aF and G. They represent the symmetric north-south temperature forcing and the asymmetric continent-ocean temperature forcing respectively. If westerly current and the eddies were uncoupled they are the values toward which X and Y would be driven. These two parameters bring energy into the system and the total energy is, obviously, not conserved. One can imagine the atmosphere system as one in which energy flows in through aF and G and out of the system due to dissipative processes like damping of the waves through $-Y$ and $-Z$, and damping of the westerly current through $-aX$. Thus the total energy in the system is limited, because if we look at the time derivative of the total energy : $(X^2 + Y^2 + Z^2)$:

$$d(X^2 + Y^2 + Z^2)/dt = \frac{-1}{2}[a(2X - F)^2 + (2Y - G)^2 + (2Z)^2 - (aF^2 + G^2)] \quad (13)$$

We can see that by putting the right hand side of equation (13) to zero we define a ellipsoid surface E, in phase space. The derivative of the total atmospheric energy is zero on E and negative outside it. If now there is a finite sphere S, centered on $(0, 0, 0)$, and completely enclosing E, all points in parameter space outside of S will eventually penetrate S and remain inside. This is also the finite volume to which all attractors are confined. So it also follows from equation (13) that the total energy stored in the variables : $(X^2 + Y^2 + Z^2)$ is bounded, because F and G are bounded.

By equating the left-hand sides of equations (10) – (12) we can determine the steady states and find that X, Y and Z obey:

$$\begin{aligned} Y &= \frac{(1-X)G}{1-2X+(1+b^2)X^2} \\ Z &= \frac{bGX}{1-2X+(1+b^2)X^2} \end{aligned}$$

$$a(F-X)(1-2X+(1+b^2)X^2)-G^2=0 \tag{14}$$

Special cases :

If $F=0$ and $G=0$ then : $X=0, Y=0, Z=0$
If $F\neq 0$ en $G=0$ then : $X=F, Y=0, Z=0$

Where if $F<1$ gives a stable solution because $XY-Y<0$. and $F>1$ gives an unstable solution because $XY-Y>0$ causing Y to grow, which in turn causes Z to grow. And the solution will obey (14).

From (10)– (12) we also find that for V, a volume of infinitesimal proportions, holds :

$$\frac{dV}{dt}=V\vec{\nabla}\cdot(\dot{X},\dot{Y},\dot{Z})=-V(a+2-2X) \tag{15}$$

Where the right hand side of (15) is negative only when $X<1+\frac{1}{2}a$. Thus it is not assured that small volumes will always shrink to zero. Later on when regarding Lyapunov-exponents with the coupled model this becomes obvious immediately from the results.

2.3 The coupled equations

The ocean and atmosphere models are now coupled. A sketch of the coupled system can be found in figure 2.3. The explanation of the coupling terms and associated parameters follows the equations below. The atmospheric equations become :

$$\dot{X} = -Y^2-Z^2-aX+a(F_0+F_1T) \tag{16}$$
$$\dot{Y} = XY-bXZ-Y+G_0+G_1(T_{av}-T) \tag{17}$$
$$\dot{Z} = bXY+XZ-Z \tag{18}$$

And the oceanic equations :

$$\dot{T} = k_a(\gamma X - T) - |f|T - k_w T \tag{19}$$
$$\dot{S} = \delta_0 + \delta_1(Y^2 + Z^2) - |f|S - k_w S \tag{20}$$
$$f = \omega T - \xi S \tag{21}$$

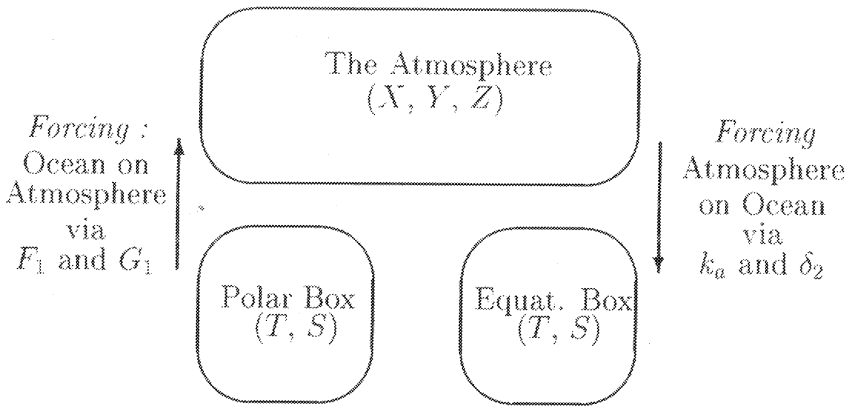

Figure 3: The coupled system

Deriving the parameter values from physical quantitative reasoning proved to be impossible, see section 2. The ocean however, does directly represent physical quantaties. So we would like to see the forcing of the ocean in corresponding quantitative terms. I will first discuss the forcing of the ocean by the atmosphere. How one should parameterize the forcing of the atmosphere by the ocean is less obvious, so another approach was taken to solve this.

2.3.1 Atmospheric forcing

The atmosphere forces the ocean through a relaxation of the ocean temperature towards the temperature of the atmosphere, in this case the difference between pole and equator air temperature. And also through an effective water flux difference of the ocean through the atmosphere. The parameter sizes are chosen rather arbitrarily, since it is hard to do anything but qualitative modelling of these processes. As a starting point for the way in which the models should be coupled Roebbers reasoning was followed (Roebber 1995). Below follows a discussion of the various processes :

The strength of the westerly current relates directly to the meridional temperature gradient. Roebber supposes that the relation is linear, and therefore he defines the restoring (atmospheric) temperature difference (T_{at}) by : $T_{at} = \gamma X(t)$. The size of γ is determined by empirical considerations i.e. its average value corresponds with the scale found in nature. I have chosen to put γ at the value of 30 so, since the average of X is approximately 1, the atmospheric north-south temperature difference is put at 30 degrees. The effect of precipitation, here in the form of an equivalent salt flux, is defined as :

$$Q_s(t) = Q_{runoff} + [Q_{wv}] + \tilde{Q}_{wv} \tag{22}$$

as proposed by Roebber. Where Q_{runoff} is the freshwater flux from the rivers and $[Q_{wv}], \tilde{Q}_{wv}$ are the mean and transient components respectively of the total atmospheric meridional water vapor transport by the eddies. Since the main interest went out towards coupled behaviour between the ocean and the atmosphere I will omit the first (constant) term Q_{runoff}. Therefore in the ocean evolution equation above, the term δ is replaced by : $\delta_0 + \delta_1(Y^2 + Z^2)$. Where δ_0 represents the mean component of the total atmospheric water vapor transport. It is assumed here that the water vapor transport is directly proportional to the eddy activity ($Y^2 + Z^2$) just as the heat transport in equation (24). Thus $\delta_1(Y^2 + Z^2)$ represents the transient component of the total atmospheric water vapor transport.

The size of the parameters determines both the relative scale of the oceanic processes, and the timescale on which these processes occur. The time-scale of the atmosphere was maintained (one unit equals five days). All parameters were scaled by comparison of the size (quantities displayed with accent, below) of the above processes with an estimate of the size of the diffusion between pole and equator of the ocean: $\acute{k}_w$ (estimated at : $5.3 * 10^5 (m^3/s)$). So the relative sizes of the oceanic parameters are correct. Then we express the timescale involved with this process in terms of the atmospheric timescale. Roebber had estimated the diffusive timescale of the ocean boxes at 500-1000 years. So the diffusion coefficient k_w (which contains the relative size of the process with respect to the whole of the ocean mass, defining the timescale of the process) in the coupled equations was given the value of 1/750 years in the atmospheric timescale : 1/(750*73). Similarly the diffusive timescale of heat exchange between the ocean and the atmosphere was estimated at 75 years, thus k_a equals : 1/(75*73). All the other processes (parameter values) where scaled with respect to this timescale :
internal diffusion : $k_w = 1/(750 * 73)$
temperature relaxation : $k_a = 1/(75 * 73)$
water flux difference between pole and equator : $\delta = \frac{\acute{\delta}}{\acute{k}_w} k_w$
temperature forcing : $\omega = \frac{\acute{\omega}}{\acute{k}_w} k_w$
salinity forcing : $\xi = \frac{\acute{\xi}}{\acute{k}_w} k_w$
The values have been based on those in Roebbers article, although he used a three

box ocean model. I simply divided the volume of the (third) deep ocean box between both two (surface) boxes. It can be shown that the dynamics of a three-box model are essentially the same as those of a two-box model (see : Lendering 1992). However, by chosing Roebber's "realistic scaling", the ocean has only one regime of flow. It can only develop poleward flow, see figure 4. The corresponding parameter values

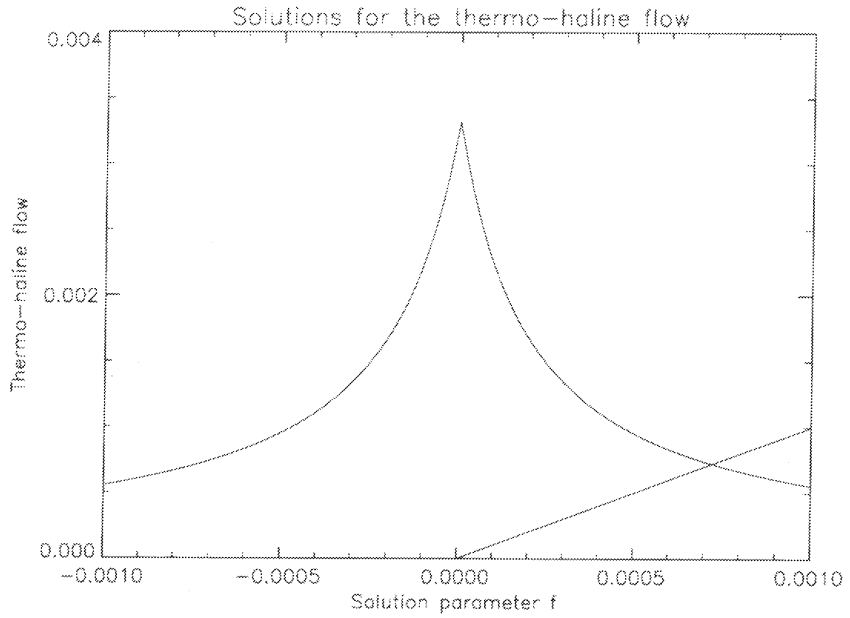

Figure 4: Solutions of the thermohaline flow ; Roebbers scaling.

are in table 1.

2.3.2 Oceanic forcing

The ocean, in its turn, forces the atmosphere via the parameters F_1 and G_1. The way this is modelled here follows Roebber qualitatively but not quantitatively. Also periodic (seasonal) terms that Roebber added have been neglected. The coupling via F_1 and G_1 is chosen in such a way that the atmospheric parameters are in the "chaotic window" (see Anastassiades 1995). According to L. Anastassiades there is a probable window in (F,G)-space for which the atmosphere model displays chaotic behaviour. The window borders are set by $8.0 \leq F \leq 8.5$ and by $1.0 \leq G \leq 1.1$. When this "window" in parameter space is investigated in more detail, it shows that it is in fact broken up by regions that give rise to periodic behaviour. We replace F in the atmospheric equations by $(F_0 + F_1 T)$. Which thus takes into account the oceanic temperature anomaly (T) contribution to the meridional temperature

a	0.25	b	4.0
F_1	$0.5 \cdot 10^{-2}$	G_1	0.01
F_0	8.0	G_0	1.0
k_a	$0.18 \cdot 10^{-3}$	k_w	$0.18 \cdot 10^{-4}$
δ_0	$0.78 \cdot 10^{-6}$	δ_1	$0.96 \cdot 10^{-7}$
ω	$0.13 \cdot 10^{-3}$	ξ	$0.11 \cdot 10^{-2}$
T_{av}	30.0	γ	30.0

Table 1: The used parameters

gradient. The parameter G is replaced by $(G_0 + G_1(T_{av} - T))$, where T_{av} is an average temperature anomaly. According to Roebber the zonal gradient in diabatic heating (G) should increase with increased high latitude ocean temperature[1]. And since the ocean temperature anomaly equals the temperature in the equatorial box minus the temperature in the polar box ($T = T_2 - T_1$). The zonal gradient is taken inversely proportional to the ocean temperature anomaly. The parameters used are in table 1. Note : here δ_1 is $\delta_0/8$.

2.3.3 The energy transfer

Note that the coupling is without energy conservation, as is the uncoupled atmosphere model by itself. Thus energy flowing into the ocean from the atmosphere (via $k_a(\gamma X - T)$ and $\delta_1(Y^2 + Z^2)$) does not cause reduction of the total energy present in the atmospheric variables. In fact the feedback is positive as an increase in X causes an increase in T via the term $k_a(\gamma X - T)$ in equation (27). Also an increase in T causes an increase in X via the term aF_1T in equation (24). In the same way the energy put into the atmosphere (via aF_1T) does not result in loss of the total oceanic energy. The feedback is very small however, compared to diffusive processes in the atmosphere. The boundedness of the total energy can be proven rigorously for the given parameters, but below I will give an outline of the "physical reason". Both models have a constant driving term that approximately cancels the internal diffusive processes. The ocean in its state of positive flow, is driven entirely by the atmosphere. Thus energy fed into it by the atmosphere is balanced by internal diffusion. In the atmosphere the feedback from the ocean is much smaller than the forcing of the constant terms (because F_1 is small). Thus the coupling as it is is equivalent to choosing a (slightly) higher constant forcing and does not cause instability. If γ or F_1 would be much bigger however, the positive feedback would give rise to instability.

[1] this is equivalent to assuming that at high latitude the ocean water temperature is higher than the temperature on the continent

3 Analysis

3.1 Numerical Integration

In order to integrate the atmosphere model a fourth-order Runge Kutta scheme has been applied, with a time step of 10^{-2} (corresponding to 1.2 hours), where a time step of one corresponds to five days. The scheme is popular for numerical simulations, because it combines both good stability and accurate results. The ocean however is much less dynamic, i.e. it is much slower than the atmosphere and can safely be integrated by the much simpler and thus faster (in terms of computer processing time) Forward Euler scheme. For the ocean also a timestep of 10^{-2} has been chosen.

3.2 Fourier analysis

The graphical program package PV-WAVE supports the possibility of making fourier transforms of offered data sets. This was used to make power spectra of the raw output. The spectrum can give some crude measure of the intensity of the chaotic nature of the signal. Reasoning that if the power spectrum of say the westerly flow displays power continuously along a range of frequencies, its behaviour must be fully chaotic, while if the spectrum displays sharp peaks in power at certain frequencies it must therefore be (quasi-) periodic or chaotic but with a small regime of possible frequencies. I found this option easy to use, and rather attractive because no problems occurred with long evolution times as with other means of labelling chaos such as fractal dimensions.

3.3 Lyapunov exponents

Another useful tool to analyse chaotic systems is the study of Lyapunov exponents and the Kaplan-Yorke dimension (which is derived from these). The Lyapunov exponents identify the growing or shrinking directions in parameter space and the rate of growth/shrinkage. As is well known two closely neighboring trajectories tend to diverge from each other exponentionally when the behaviour is chaotic. The exponential factor is a Lyapunov exponent and is also a measure of how chaotic the system is. The Lyapunov exponents are usually ordered by putting the largest in front, and then working down to the smallest (negative) Lyapunov exponent. The first Lyapunov exponent should thus be positive in the chaotic case or else there would be no diverging trajectories (or chaotic behaviour at that). There should also be negative Lyapunov exponents since else the system would not remain confined to its attractor and wander off to infinity. In an autonomous system of differential equations there is at least also one zero exponent. The maximum number of Lyapunov exponents is, of course, the number of free variables out of wich the system is constructed. This maximum number also defines the maximum of the attractor

dimension i.e. the attractor dimension is less than or equal to the dimension of the phase space spanned by all the variables. For illustration it might be useful to discuss the possible situations for just the three dimensional atmospheric system. Suppose that the system has such a parameter set that there is just one asymptotically stable equilibrium solution (a point in phase space). Then all three of the Lyapunov exponents will be negative, otherwise it would not be a stable equilibrium. Because if the solution is stable an infinitesimal perturbation, in any direction, will always end on the stable point in phase space. Thus there is 'shrinkage' in all directions. For a stable limit-cycle the combination of exponents would be one zero (in the direction of circumference), or the cycle would grow or shrink in time. And two should be negative exponents (corresponding with shrinkage near the cycle in the directions perpendicular to it). If the trajectories in parameter space lie on a stable toroidal surface the combination is two zero exponents and one negative. Finally for a chaotic system the combination of exponents is one positive, one zero and one negative. The corresponding attractor dimensions are : zero for a fixed point ; one for a limit-cycle ; two for a torus ; and smaller than three for a strange attractor. A way to define the attractor dimension is by calculating the so-called Kaplan-Yorke dimension. It can easily be calculated from the Lyapunov exponents via the following formula :

$$D_{KY} = j + \frac{\Sigma_{i=1}^{j} \lambda_i}{|\lambda_{j+1}|}, \tag{23}$$

where $\lambda_1 \geq \lambda_2 \geq \cdots \geq \lambda_n$ are the ordered lyapunov exponents and j is the integer defined by the following conditions :

$$\Sigma_{i=1}^{j} \lambda_i \geq 0$$

and

$$\Sigma_{i=1}^{j+1} \lambda_i \ < 0$$

In our coupled model experiments it will be shown that the Kaplan-Yorke dimension of the strange attractor ranges between 4.0 and 4.5, perhaps that other investigations will show that the attractor dimension can be higher or lower. I found only one positive Lyapunov exponent in the case of a strange attractor. And it proved worthwhile to keep track of this exponent during my investigations. The algorithm with which the Lyapunov exponents where determined was derived from Wolf *et.al.* 1984. This paper also contains a FORTRAN program to determine (while integrating) the Lyapunov spectrum for the Lorenz 1963 model. For a plot of the time-dependent behaviour of the Lyapunov exponents and the Kaplan-Yorke dimension in the case of fully chaotic behaviour see figure 5 (for the set : $(F_1, G_1) = (3.5, 1.0) * 10^{-2}$).

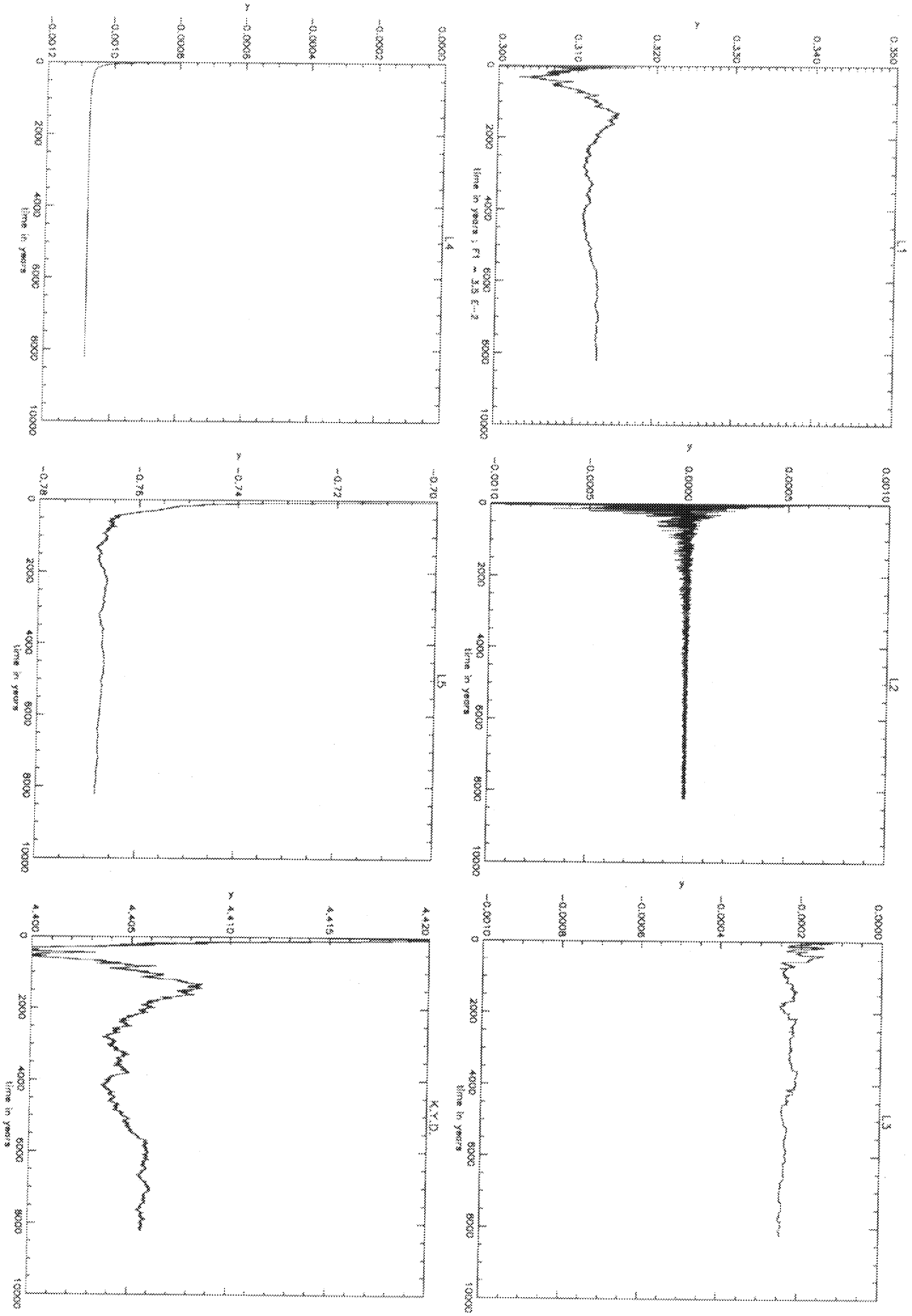

Figure 5: The five Lyapunov exponents (L_1–L_5) and the Kaplan-Yorke dimension (D_{KY}) (during fully chaotic behaviour).

3.4 Projections

In order to visualize the shape of the attractor, projections were made of the four "active variables" namely X, Y, Z and T. The variable S displays virtually no activity and as will be shown later did not contribute much dynamics of the system. The projections were made on the Y, Z-plane and on the X, T-plane respectively. This is nothing more than a way of displaying the observed data, but it proved to be very clarifying when trying to maintain a picture of the attractor shape and range. The plots were made by using 10,000 points, each being separated from the other by approximately 2.5 days.

4 Experiments

In this section both the experiments and the results that follow will be discussed. The effect of coupling on the atmospheric model was investigated at first by simply varying the coupling strength from ocean to atmosphere. This was performed by varying the parameters F_1 and G_1. The experiment was started by putting F_1 and G_1 equal to zero, thereby removing the oceanic forcing on the atmosphere. F_1 and G_1 are called the feedback parameters. When they are non-zero, they are responsible for the forcing on the atmosphere by itself via the ocean. Since the ocean is driven entirely by the atmosphere and constants. The state of the atmosphere is chaotic, and its behaviour is described in the respective section below. The forcing on the ocean by the atmosphere is retained. As monitoring parameters the strength of the westerly current for the atmosphere X and the pole-equator temperature difference for the ocean T were chosen, since the coupling depends most strongly on these. Then the feedback was introduced via either F_1 (at the value $1.2 * 10^{-2}$) or G_1 (at the value $1.0 * 10^{-2}$). And when coupling was thus introduced, the value of the other parameter (either G_1 or F_1) was varied. So the value of F_1 was being put (arbitrarily) at $1.2 * 10^{-2}$ when G_1 was varied. And G_1 was put to $1.0 * 10^{-2}$ when F_1 was varied. The area in wich I varied F_1 and G_1 is spanned by : $0 < F_1 < 8.0 * 10^{-2}$ and $0 < G_1 < 8.0 * 10^{-2}$. In the investigated range, there are stable stationary solutions and periodic solutions and there is chaotic behaviour. In the sections below the respective behaviour will be discussed in this order and also the behaviour when the system underwent transitions between regimes. The transitions between the various regimes proved to be the most interesting part of parameter space, because here the system is most sensitive and the effect of coupling can be observed. For an overview of behaviour versus varying F_1 or varying G_1 see figure 6.

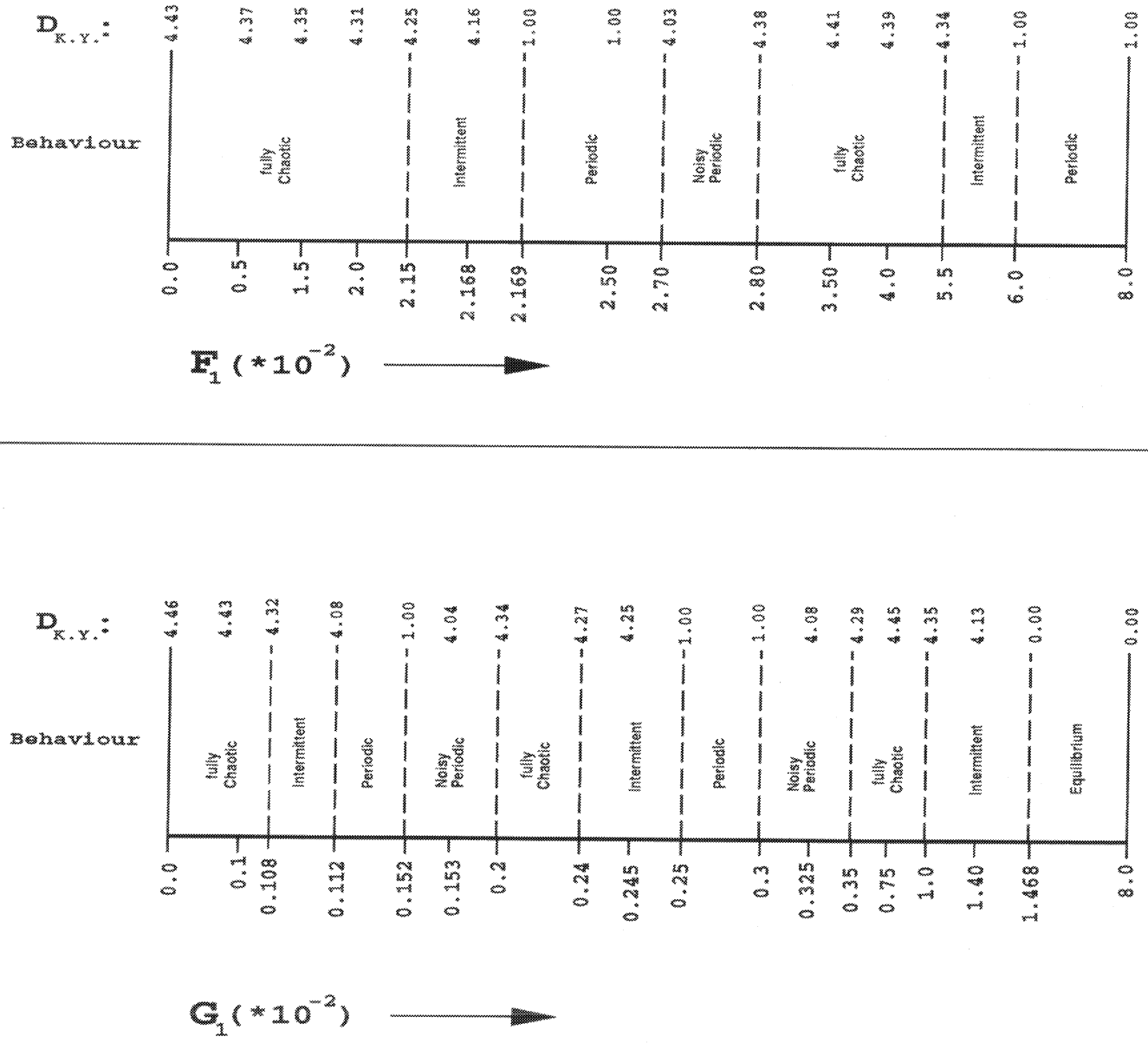

Figure 6: The behaviour and corresponding Kaplan-Yorke dimension for various values of F_1 or G_1.

4.1 Equilibrium solutions

The equilibrium solutions can be found directly from the coupled equations themselves, via :

$$\dot{X} = 0 = -Y^2 - Z^2 - aX + a(F_0 + F_1 T) \quad (24)$$

$$\dot{Y} = 0 = XY - bXZ - Y + G_0 + G_1(T_{av} - T) \quad (25)$$

$$\dot{Z} = 0 = bXY + XZ - Z \quad (26)$$

$$\dot{T} = 0 = k_a(\gamma X - T) - |f|T - k_w T \quad (27)$$

$$\dot{S} = 0 = \delta_0 + \delta_1(Y^2 + Z^2) - |f|S - k_w S \quad (28)$$

This is a tricky set of equations to solve, but luckily there are a few numerical packages available that can approximate the solutions quite accurately. In the parameter range that was investigated there was a certain combination of (F_1, G_1) for which there occurred a transition from chaotic behaviour towards a stable equilibrium solution when G_1 was increased (see section 4.4.2). This stable equilibrium solution can also be found by the use of an equation solving routine in MAPLE. For lower values of G_1, where the behaviour was intermittent in the numerical simulations, stable equilibria could also be found with MAPLE. This transition is discussed in more detail in section 4.4.2

4.2 Periodic Behaviour

There are limit-cycle solutions for different values of both F_1 and G_1 and there are many variations in which the limit-cycles appear within this coupled model. However their shapes are very similar and also the scenarios by wich the variable values are varying periodically, are alike. I will try to analyse the processes involved by discussing a simple limit-cycle for the (F_1, G_1) set $(1.2{*}10^{-2}, 0.3{*}10^{-2})$. The cycle is displayed in the form of two projections in figure 7. One projection is performed on the (Y, Z)-plane. The other projection is performed on (X, T)-plane. Note the small variation in T. The salinity displays minute variation (less than $1{*}10^{-7}$ (unit)) and can thus be considered constant at $1.328 * 10^{-3}$ (unit).

We know from the equations that there is energy transfer from X to Y and Z at the expense of X. This can be retraced in the experimental data. Let us first look at the time dependent relation between X and the energy E_w contained by the atmospheric waves : $(Y^2 + Z^2)$. Both are displayed in figure 8. We see that X grows as a result of the terms F_0 and $F_1 T$. Via the energy exchange between the westerly current and the waves, also the energy stored in the waves starts to grow. The increase in wave-energy causes a decrease in X because of the negative terms associated with wave-energy (see equation (10)) the westerly current strength decreases as energy is transformed into the waves. The wave-energy continues to rise and the westerly current strength continues to fall. Until the energy stored in

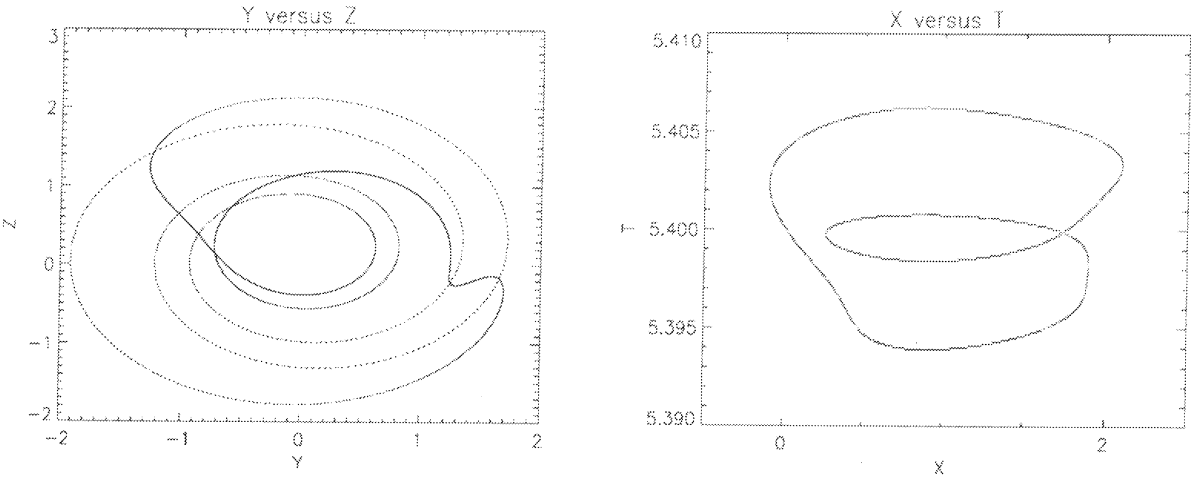

Figure 7: The limit cycle displayed in two planes in parameter space, for $(F_1, G_1) = (1.2, 0.3) * 10^{-2}$.

the waves reaches its maximum and starts to decline also. This because there is a decrease in the energy supplied by X and because the diffusive terms take energy out of the system. When the wave amplitude has reached a small enough value, X gets the opportunity to rise again. It also starts giving off energy to the waves until they climb out of their minimum. And the cycle repeats. Note that the cycle has a period of approximately 1.5 months. If one looks again at figure 7 and imagine that the cycle is in counterclockwise direction. One can see Y and Z moving on a closed curve with a radius varying according to the energy that is fed by X and the constant term G_0 and the ocean dependent term $G_1 T$. Thus it's always lagging behind the latest development in X. This is a very crude description, as can be seen the cycle displays more structure (the S-like shape around $Y = 1.3$) which originates from phase lock effects from parameter G_0. There are also dissipative and constant terms wich might be responsible for this, but it was the interplay between X and Y, Z which I wanted to analyse.

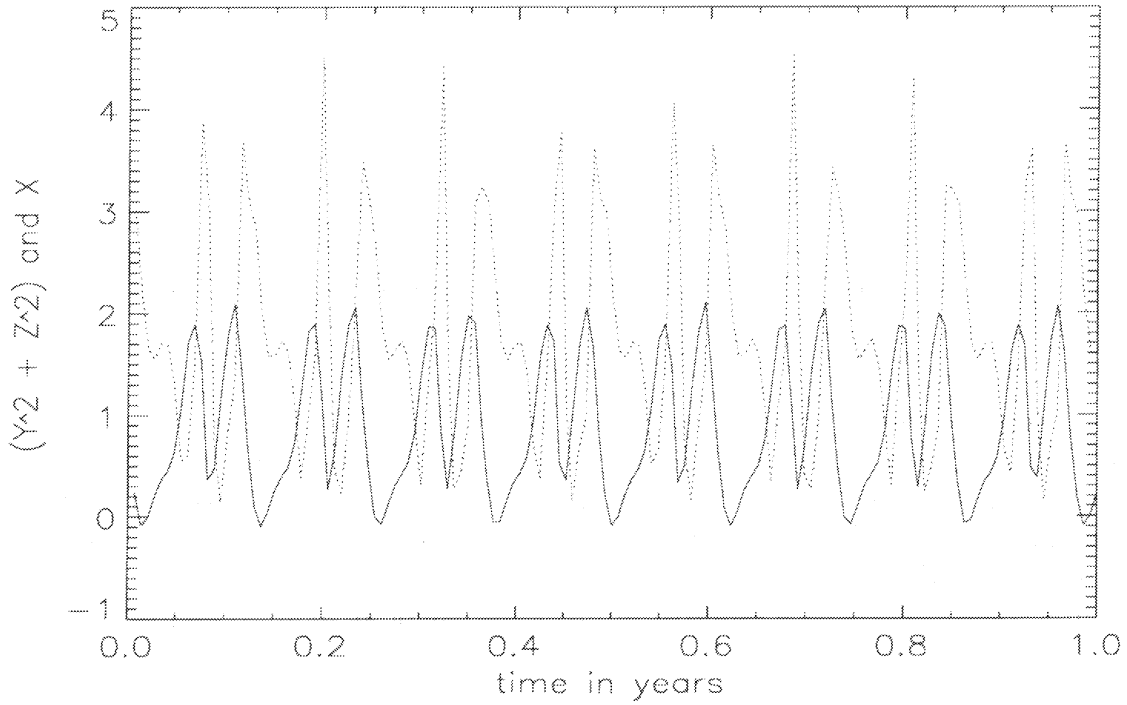

Figure 8: X (full line) and the energy stored in the waves E_w (dotted line) as a function of time, for $(F_1, G_1) = (1.2, 0.3) * 10^{-2}$.

This interplay differs from the interaction between X and the ocean temperature T, where there is no energy conservation as such (see the coupled model description above). Just as the atmospheric energy contained by Y and Z, the ocean temperature anomaly is lagging behind the westerly current. And the dynamics involved appear to be very simple as shown by the-limit cycle in figure 7. This limit-cycle is traversed in counterclockwise manner. The same data as time dependent signal can be seen in figure 9. As we know from the equations, the oceanic temperature

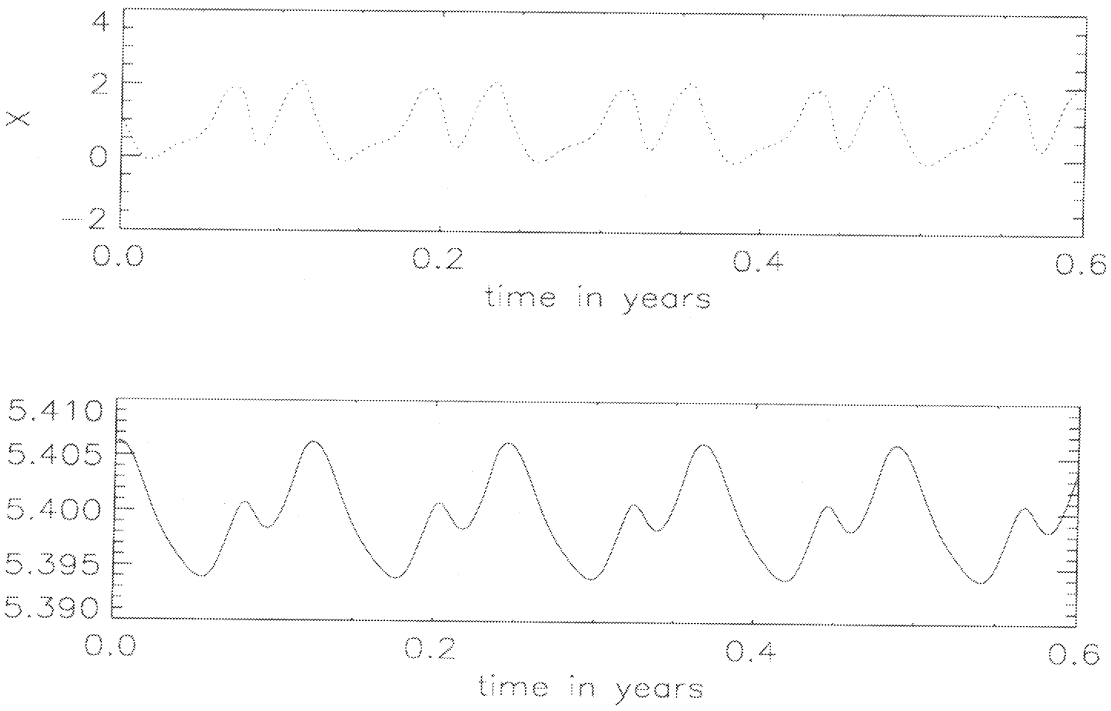

Figure 9: X and T as a function of time, for $(F_1, G_1) = (1.2, 0.3) * 10^{-2}$

anomaly follows the trail of the westerly current strength, it behaves like a time integrated value of X (with diffusion of course). And the scenario is like a lazy dog (T) slowly trudging behind its master (X), see figure 7. Note also the small amplitude in the oceanic signal, as said before the ocean is a slow system and signals with a short time-scale like that of the atmosphere cause little reaction. This seemingly passive behaviour of the ocean was checked by forcing the atmosphere with the time averaged value of the ocean-temperature as a constant in time. This resulted in the same limit-cycle behaviour. The coupling from the atmosphere to the ocean was maintained for comparison and it showed that the produced signal was exactly the same. The time-dependent behaviour looks exactly like figure 9 above. For an example of a power spectrum of X in both the case with and without feedback see

figure 10. Thus in the periodic case the oceanic dynamics are probably unimportant.

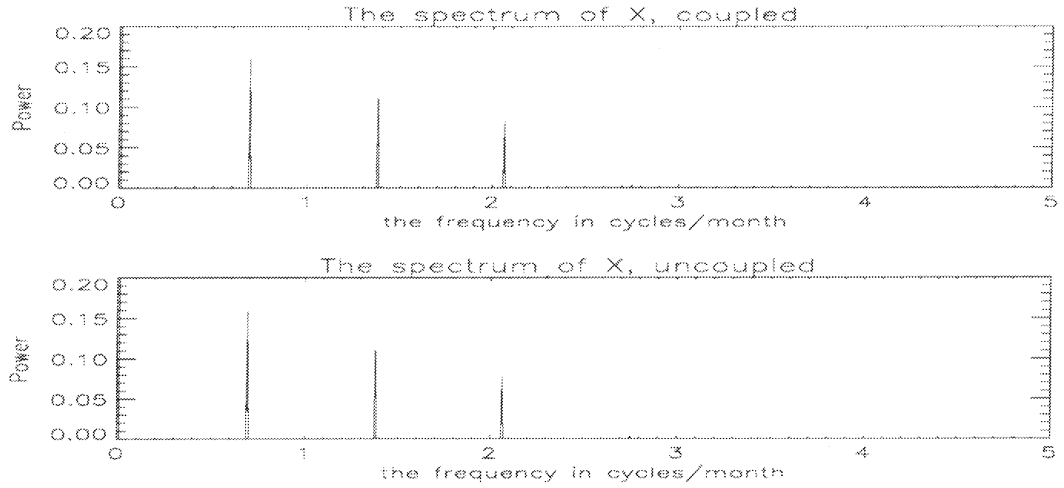

Figure 10: The frequency spectrum of X (in cycles per month) during periodic behaviour, both with and without feedback for $(F_1, G_1) = (1.2, 0.3) * 10^{-2}$.

So apparently it is the parameter X that forces Y,Z,T above their minimal values. And it is the parameter F_0 that acts as the main forcing on X since the variation in $F_1 T$ due to T is very small (less than $1.7 * 10^{-4}$ compared to 8.0). However when transitions between regimes occur we shall see that the ocean plays a vital part.

4.3 Chaotic Behaviour

In this paragraph I will discuss the typical chaotic behaviour that occurred in certain areas in parameter space (see paragraph 2.3.2 : Oceanic forcing). Also in the chaotic regime the scenario described in the periodic case probably still holds, in that the ocean is still a slave of the atmosphere. This can be illustrated by figure 11. Here we see the long-time scale chaotic behaviour for the (F_1, G_1)-set : $(1.2, 0.75) * 10^{-2}$.

In this plot, in both the atmospheric and the oceanic signal, the high frequency

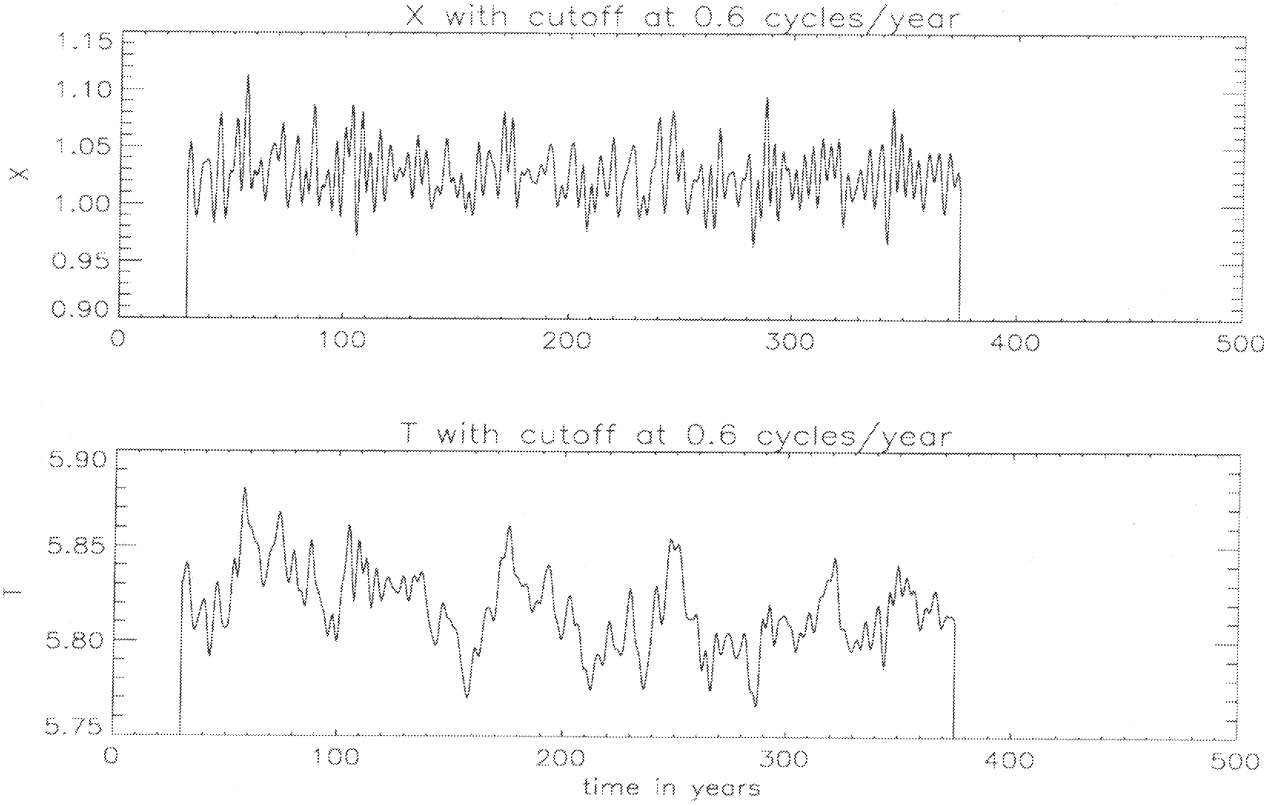

Figure 11: The filtered signals of X and T as a function of time, for $(F_1, G_1) = (1.2, 0.3) * 10^{-2}$

signals have been filtered out. Because now that there is chaotic behaviour, the atmospheric signal also contains a signal with a long time scale. We have already seen in the periodic case that the short time-scale behaviour of the atmosphere resulted in a very small response in the oceanic variables. This is to be expected since the ocean has, due to its "inertia", an averaging character. Thus we only see a clear oceanic response on the signals with a long time scale. But as can be observed from the figure also in this long time-scale behaviour the response of the ocean resembles the behaviour in the periodic regime. It follows the long time scale

trend of the atmosphere. The ocean in its turn forces the atmosphere, one would thus expect an increase in the power of low frequency signal in the atmospheric data. This effect however was not observed however (see figure 12). Apparently the atmosphere is little influenced by the ocean. First I will describe the behaviour in the

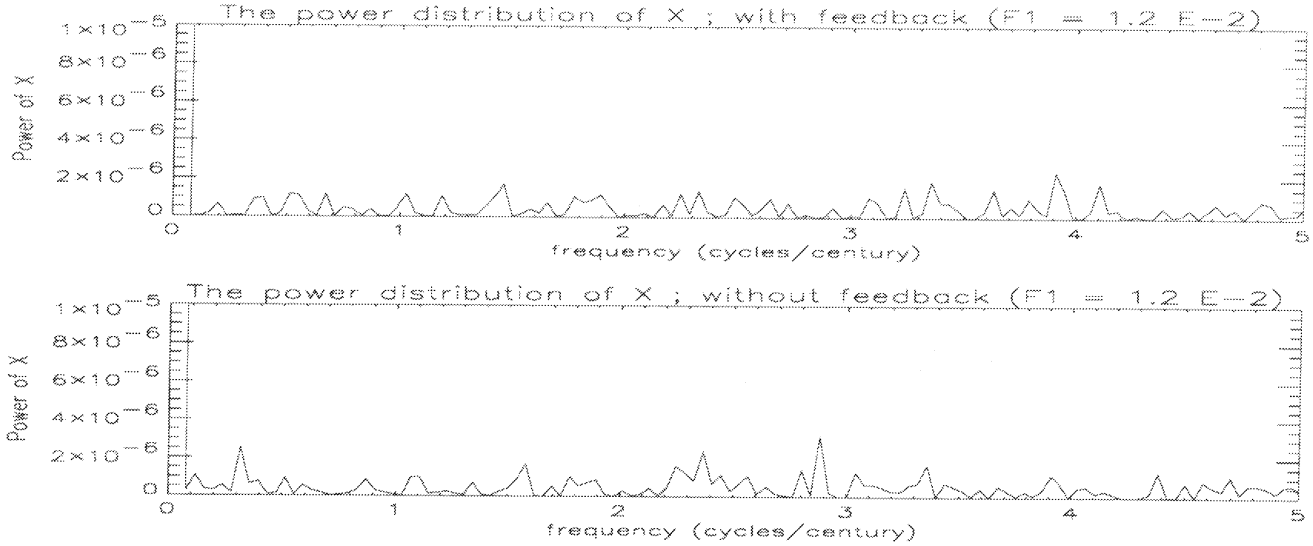

Figure 12: The low frequency part of the power spectrum of X in both the coupled and the uncoupled case.

case without feedback, or with partial feedback through only one of the parameters F_1, G_1. In this case (F_1, G_1) was set to $(0, 0)$, resulting in a system where the ocean is forced by the atmosphere but not vice versa.

4.3.1 The system without feedback

The system behaved fully chaotic, and the power spectrum of the parameter X was dense. For the Kaplan-Yorke dimension the value 4.43 was found and for the first Lyapunov exponent : 0.240. So the attractor dimension is relatively high, it showed however that this was a typical value, also for the fully coupled case, indicating fully developed chaos. The scenario in the case of periodic behaviour, also contributed to my choice of monitoring variables. It was decided to use the variable X as the monitoring variable for the atmosphere. And the variable T as a monitor for the ocean. A picture of both the oceanic T-signal and the atmospheric X-signal can be found in figure 13 with the power spectrum of the X-signal below them. The signal was then fourier-transformed and a frequency spectrum was plotted. It showed that the signal showed power at a large range of frequencies (see section : 4.3.1).

As can be seen in figure 13 the spectrum of X has three dominant frequencies. But there is also some power in the low frequency signal. It is the low frequency atmospheric signal that has the greatest response from the ocean. The spectrum

of the oceanic signal is displayed in figure 13 at the bottom. I used the half-year averages of the signals, because when one wants to observe the signals on longer timescales the half-year averages give a much clearer view on what is going on. So a plot of the averaged signals can be found in figure 14. Beside the signal itself it is also illustrative to observe the power spectrum of this signal. Below both signals is the spectrum of the averaged atmospheric signal. The cutoff at 100 cycles per century is caused by the half-year averaging. This picture is characteristic of the chaotic signals found for other values in the (F_1, G_1) set. However there is a change in the spectrum, a rise in the power in varying frequency bands, for different moments and different parameter sets (see the following section).

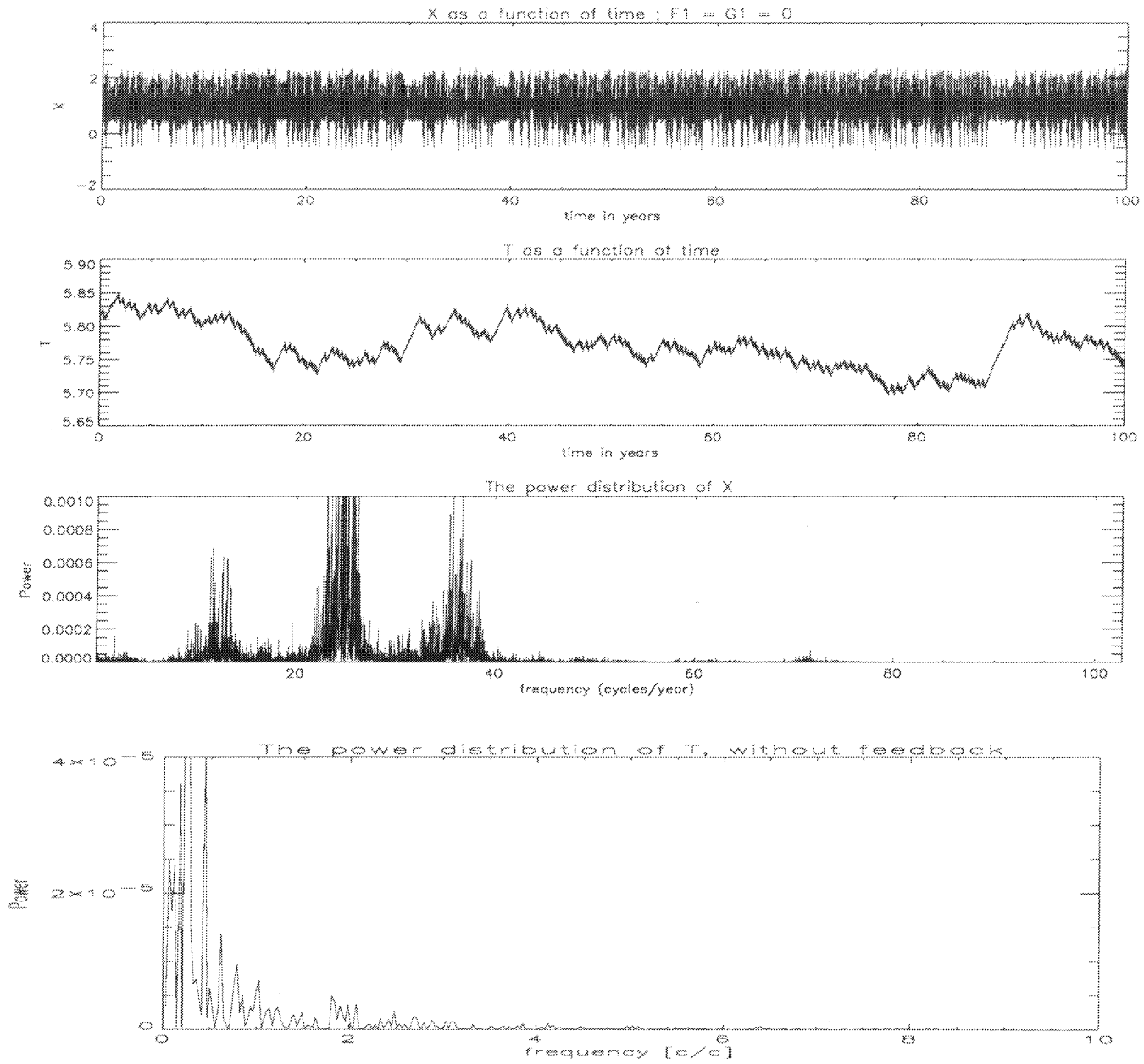

Figure 13: The uncoupled signal X,T as a function of time, and the frequency spectrum of X (cycles per year) and T (cycles per century) ; $((F_1, G_1) = (0, 0))$.

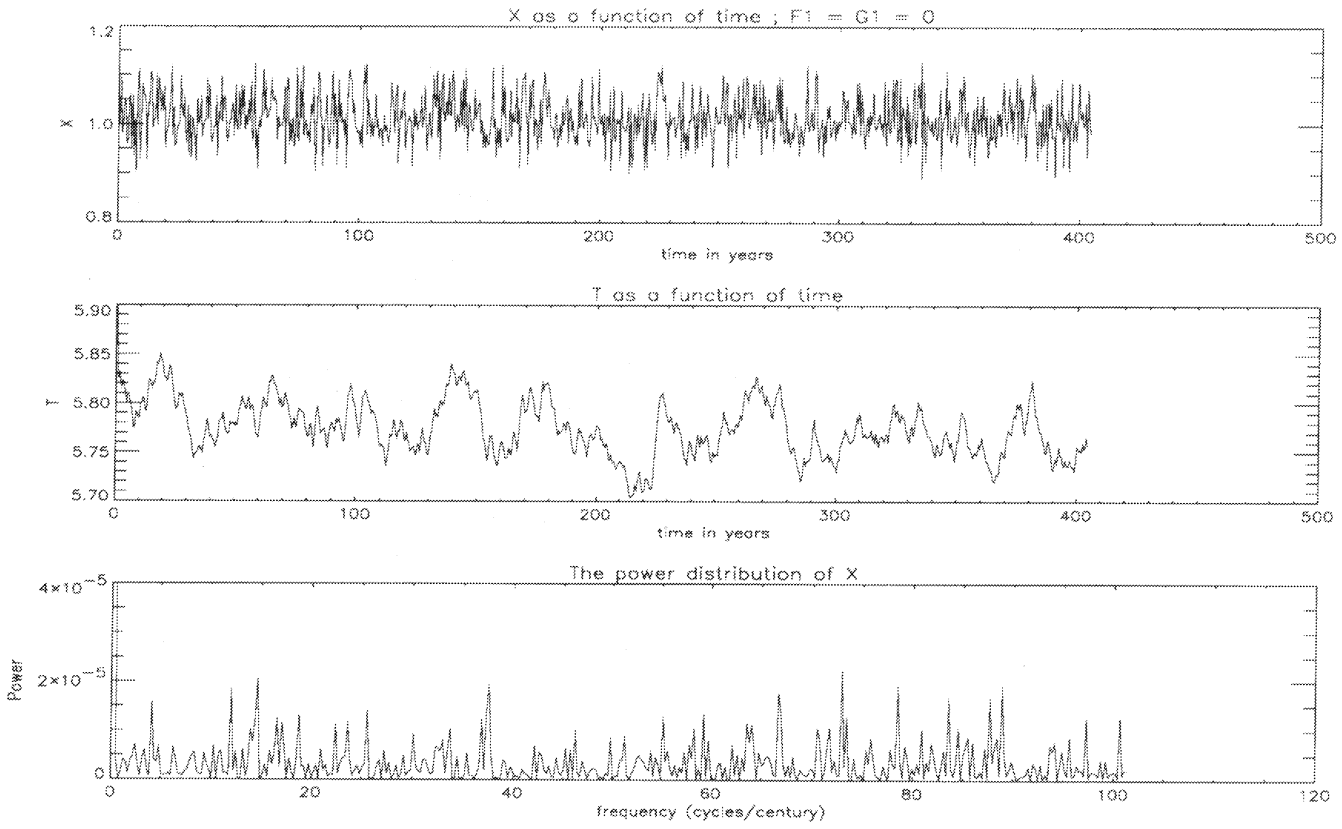

Figure 14: The uncoupled signal : the half-year average of X,T as a function of time and the spectrum of the averaged X ($(F_1, G_1) = (0, 0)$).

(F_1, G_1)	$\overline{X}$	$\overline{T}$	$\Delta\overline{X}$	$\Delta\overline{T}$
$(0,0) * 10^{-2}$	1.0154	5.7817	0.0012	0.0038
$(1.2,0) * 10^{-2}$	1.0306	5.8301	0.0015	0.0044
$(0,1.0) * 10^{-2}$	0.9770	5.6590	0.0019	0.0063

Table 2: The averaged values and differences between feedback and no feedback.

4.3.2 Introducing the feedback

We will now introduce the feedback, first by making G_1 nonzero (while $F_1 = 0$). Then by making F_1 nonzero (while $G_1 = 0$). When feedback was introduced by making G_1 nonzero a change occurred in the averaged signal.

In the case of $(F_1, G_1) = (0, 1.0) * 10^{-2}$ the average of X is lower, though it also displays more extreme values. That the average is made lower is not very strange, since by feeding power to Y (see equation (24)), one effectively damps X. The power spectrum of the averaged X-signal in this case displays an increase in power around 100 cycles/century (c/c). This effect is not caused by the feedback itself, but by an effectively increased G_0. This was proven by forcing the atmosphere with the averaged value of T (aquired from the run with feedback) as a constant in time, thereby removing the feedback. One sees the same shift in power towards the 100 c/c. The averaged value however differs from the system with feedback. The averaged T is slightly (but noticably) higher in the case without feedback then in the case with feedback. The averaged values for X, T and the differences between these values for both the case with and without feedback are displayed in table 2 (for $(F_1, G_1) = (0,0)$ see below). The Kaplan-Yorke dimension has the slightly increased value of 4.44.

By introducing the feedback through the parameter F_1 using the set $(F_1, G_1) = (1.2, 0) * 10^{-2}$ one sees an increase of the average of X, also not surprising, since the term $(F_0 + F_1 T)$ directly forces X (see equation (24)). The increase in power in the signal of the averaged X is now at around 50 c/c. This effect also occurred in the system without feedback, the atmosphere being forced with a constant averaged T-value in time. But again the averaged values of the two monitoring variables in the case with feedback are lower then those in the case without feedback. Both are displayed in table 4.3.2. The Kaplan-Yorke dimension has the value : 4.46, so there has been some increase.

For comparison also the difference between the averaged values of X and T between two runs with $(F_1, G_1) = (0,0)$ is displayed. Remarkable in both cases in which feedback was introduced, is that such a small change in the parameters, can still cause a visible change in behaviour. Compare for $F_1 = 1.2 * 10^{-2}$, with the constant parameter F_0 : 8.0, the parameters differ a factor thousand.

After introducing the feedback through either F_1 or G_1 the other parameter is increased. The Kaplan-Yorke dimension varies with changing feedback strength. In both the experiments with increasing G_1 and increasing F_1, increasing the coupling strength generally results in a decrease in the first Lyapunov exponent. Which in turn causes a decrease in the Kaplan-Yorke dimension. This effect continues until we come close to a transition, in which the coupled system moves to a periodic attractor. In these transitional regions in parameter space the parameter sensitivity can be enormous. Another notable feature of these transitional regimes is the large decrease in the positive Lyapunov exponent. There are many regime transitions in the small area that is investigated, but there are probably only two scenarios for these transitions:

1. The transition from chaotic to either periodic behaviour or a stable point solution, via intermittency.

2. The transition from periodic behaviour to chaotic behaviour, via bifurcation.

The description of the systems behaviour close to the transition point can be found in the respective paragraph below.

4.4 Transitions between regimes

4.4.1 The transition from chaotic to periodic behaviour

The transition from chaotic behaviour to periodic behaviour is of the intermittent type, where the behaviour in the intermittent intervals is like the behaviour of the periodic signal when the coupled model has finally reached the stable periodic attractor. The transition occurred around $F_1 = 2.17 * 10^{-2}$ when F_1 was increased. When we look at the case $F_1 = 2.15 * 10^{-2}$ intermittency has already set in, the intermittent intervals lasting about 15 years. During these intermittent intervals the averaged atmospheric signal is lower than during chaotic behaviour. So in the "periodic" years also the ocean temperature anomaly drops in value (see figure 15). The Kaplan-Yorke dimension has dropped to a value of 4.25, the first Lyapunov exponent is about 0.169. When F_1 is increased so does also the length of these intermittent periods. For F_1 =(2.164 ; 2.168 ; 2.169)*10^{-2} the periodic times last for (20 ; 32 ; 45) years respectively. By this increase in the intermittent intervals the ocean temperature anomaly gets the opportunity to relax to lower values. However the coupled system does not yet have the opportunity to settle on the periodic attractor. It will return to chaotic behaviour when the oceanic signal comes near to some minimal value. This is in contrast with the onset of the periodic interval ,which takes place at apparently indiscriminate values of T. For the above mentioned values of F_1 the values for the Kaplan-Yorke dimension are : (4.20 ; 4.16 ; 1) (the first Lyapunov exponent has values : (0.153 ; 0.135 ; 0). For the last F_1 value periodicity

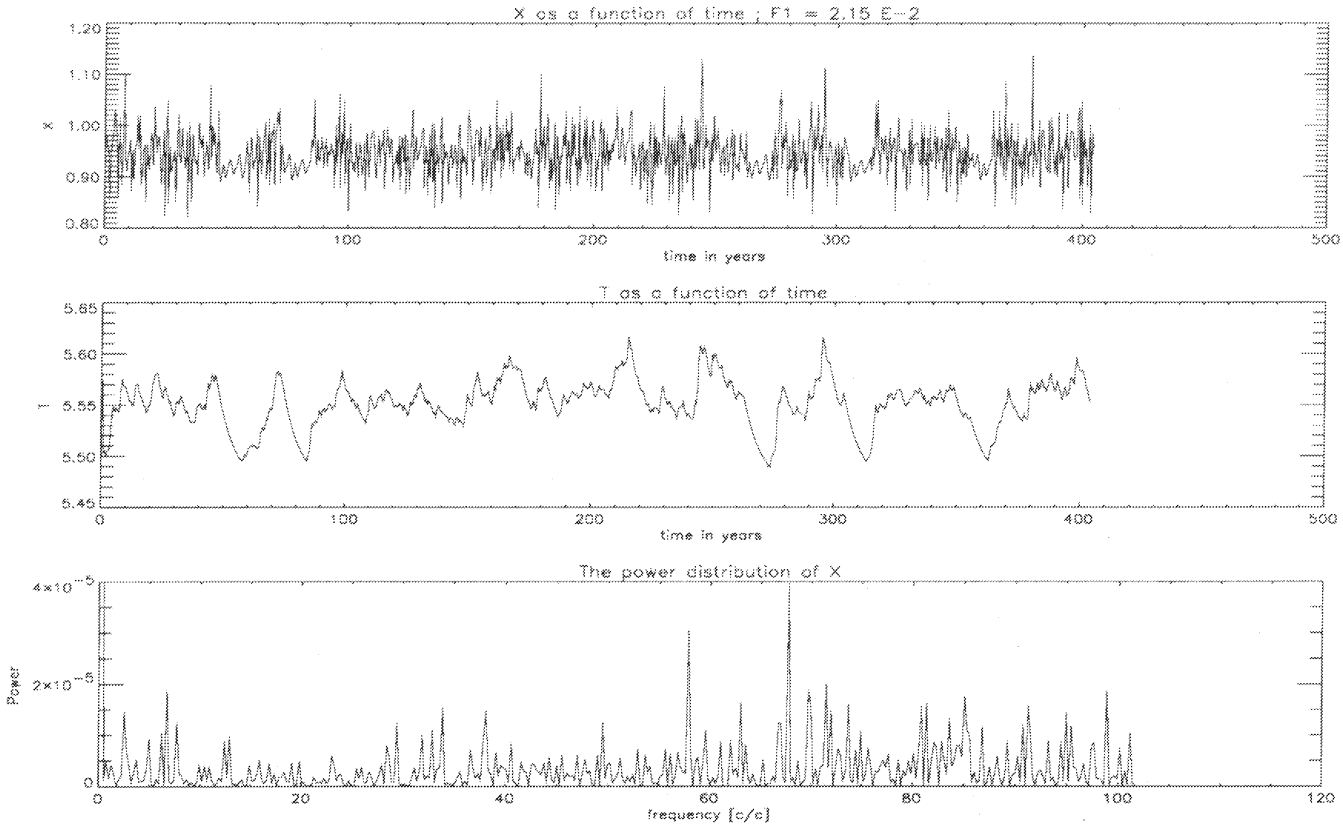

Figure 15: The averaged intermittent signal as a function of time, for $(F_1, G_1) = (2.15, 1.0) * 10^{-2}$.

sets in and stays, after about 1150 years. The time-run is shown in figure 16 (note the different time-scale). On variation of the initial condition for the last F_1 value it showed that this intermittent state can last for largely varying timespans. It ranged from about less than a year to more than 32.000 years (the experiment was stopped after 32.000 years).

Further experiments where conducted. When those initial conditions which gave intermittent behaviour for more than 32.000 years where slightly perturbed (as small as possible within the accuracy of the program (16 digits)), i.e. a slightly different initial condition was chosen, the intermittent behaviour lasted never more than a few hundred years. We can conclude that the initial conditions from which intermittent behaviour lasts more then 32.000 years are defined as very small areas or points in phase space. For this situation one might speculate in the following way : In the phase space of the coupled model there is one periodic attractor that has become stable for our specific (F_1, G_1)-set. In the attraction-basin of this periodic attractor are thin tubes for which the system does not collapse towards the periodic attractor.

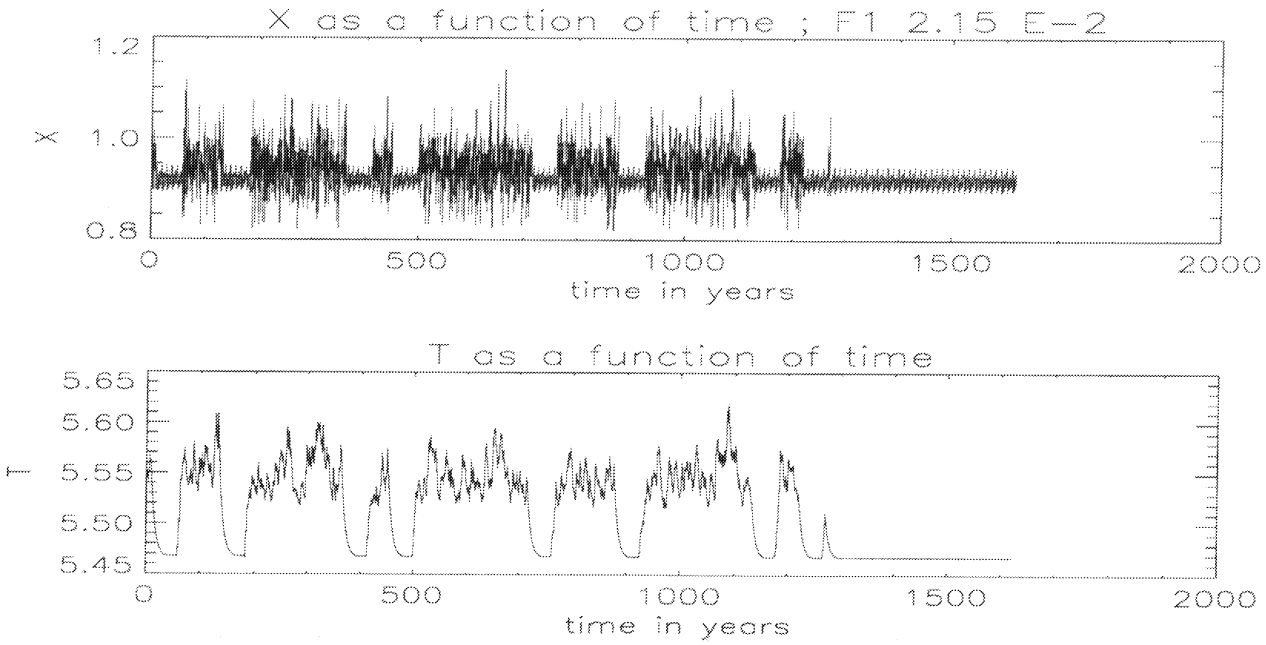

Figure 16: The averaged intermittent signal, the transition towards periodic behaviour takes place after 1300 years.This is for $(F_1, G_1) = (2.169, 1.0) * 10^{-2}$.

But in which intermittent behaviour takes place. A small [2]perturbation however will eventually move the system out of these tubes and on to the periodic attractor. Another remarkable phenomenon occurs when the integration scheme of the ocean is changed. Usually it makes little difference whether the ocean is integrated via the usual Forward Euler scheme, or the more complicated Runge-Kutta 4-th order scheme. But in the sensitive regime that we have entered here, it does. By changing the integration scheme to the R.K. 4-th order, the intermittent intervals last longer. In the previous sketched image it would mean that we stay longer in the intermittent tubes by the more accurate integration scheme.

Although the previous results seem to suggest otherwise, it is still not certain whether the ocean dynamics are an essential part of the coupled system. It could be that the ocean only acts as a atmosphere parameter modifier, and only its mean value is of importance to the atmospheric behaviour. The intermittent behaviour then being dictated by the atmosphere, and the ocean is just following the atmospheric signal. To investigate this the following experiment was conducted : In the 'chaotic' intervals of the intermittent behaviour ($F_1 = 2.164$, not too close to the transition towards periodic behaviour) of the system with feedback, the ocean temperature anomaly varies between the extreme values : $5.53 \leq T \leq 5.58$. Then the atmosphere was forced with a constant T-value in time for various values in this range (the system

[2]or a round-off error as a result of the limited accuracy of the computer

is now without feedback). For each of those values the atmosphere displayed limit-cycle behaviour, where the chaotic transient behaviour lasts longer for higher value of T. Thus by removing the feedback, we have also eliminated intermittent behaviour. As mentioned before, after an intermittent interval the atmosphere behaves as if fully chaotic the transition seems to occur when the ocean variable T has reached a certain (minimal) value. During the periodic behaviour the average of T is about 5.46. When the atmosphere was forced with this value, as a constant in time, it displayed only chaotic behaviour. Thus in the intermittent case the feedback is an essential ingredient for the behaviour. Where, through the feedback, the ocean induces a bifurcation in the atmosphere when it has reached the minimal value.

When we look at the oceanic signal in more detail, during an intermittent interval, we see that there is some curvature in the mean value (see figure 17). The transition to chaotic behaviour takes place at 21 years. This curvature of the signal

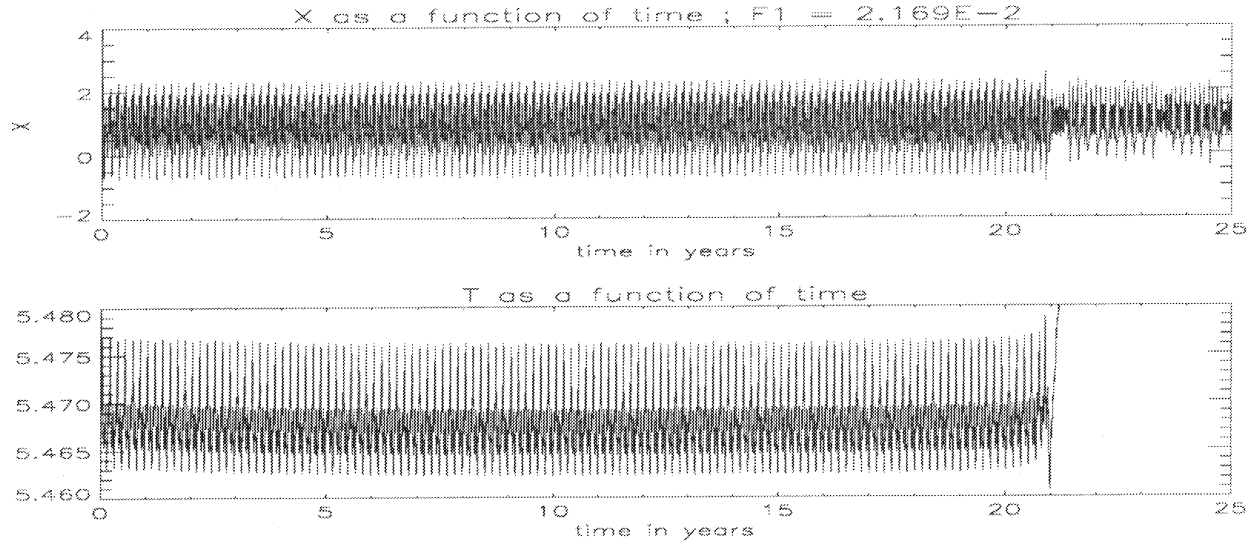

Figure 17: The signal during an intermittent interval for $(F_1, G_1) = (2.169, 1.0) * 10^{-2}$.

shows a resemblence to what is known as "type 1 intermittency" (Schuster 1984), where the intervals where the signal appears periodic are under influence by what is then called the "ghost of the limit cycle". Aptly named so, because the signal during an intermittent interval resembles the stable periodic behaviour. Note that another way of looking at this transition to a periodic attractor could be the inverse route to chaos. One would then start at the periodic attractor, decrease the value of F_1 and reach chaotic behaviour. Therefore the intermittent intervals, still resembling the periodic behaviour, would then be associated with the above mentioned 'ghost'. To further investigate the type of intermittency found here, one could determine the distribution of lengths of the intermittent intervals as a function of parameter F_1.

4.4.2 The transition from chaotic behaviour to a stable equilibrium solution

As we saw earlier we could find within our (F_1, G_1)-range a region for which the coupled system moves to a stable point attractor in phase space (the equilibrium solution). Below is a description of the transition from chaotical behaviour to the stable equilibrium. This transition is induced by increasing the parameter G_1. But before the critical value for G_1 is reached for which the system moves to a stable equilibrium, the behaviour is of the intermittent type. Where during an intermittent interval the system moves close to a stable point attractor (see figure 18). The intermittent intervals become longer with increasing G_1, until, for a critical value for G_1, the system reaches a stable point attractor. When we come close to the stable point regime in (F_1, G_1)-space, we can already notice the drop in the value of the Kaplan-Yorke dimension : $D_{KY} = 4.13$. The intermittent behaviour sets in for a value of G_1 for which a stable point solution is possible (as found with the MAPLE package), this solution is never reached however. But when the numerical experiment was started with initial conditions in close proximity to the stable equilibrium, the system moved towards, and stayed on the stable equilibrium. So although the stable attractor was not reached when starting from distant initial conditions. In analogy with the previous section : during the intermittent behaviour there was already a stable equilibrium solution. It might be interesting to investigate the domain of attraction, and see if it is indeed limited to a region close to the stable equilibrium solution. Note that the stable solution that is approached in figure 18 gives a low value for X and thus also a low value for T (just as in the case with "periodic" intermittency).

When looking at the intermittent behaviour on a longer time-scale, it seems as if there are two possible regimes of chaotic behaviour (see figure 19). The two regimes differ in the mean value of the variables and the system is switching between those two means. This is caused by a different frequency of ocurrence of the intermittent intervals. During such an interval the mean value of both X and T is much lower. Thus the regime with the lower mean would correspond with intermittent behaviour with a high frequency of intermittent intervals. The high-mean value corresponds to approximately 12 intermittent intervals per ten years, the low-mean value occurs when there are about 19 intermittent intervals per ten years. This behaviour has led to the following conjecture : By increasing G_1 we bring the coupled system into another region in phase-space that's somewhat closer to a stable point attractor. And thus does the coupled system eventually move to this stable point solution. For the lower values of G_1, for which the system was intermittent, the stable solution was also a possibility, only it lies in a region in phase-space that's rarely or never visited.

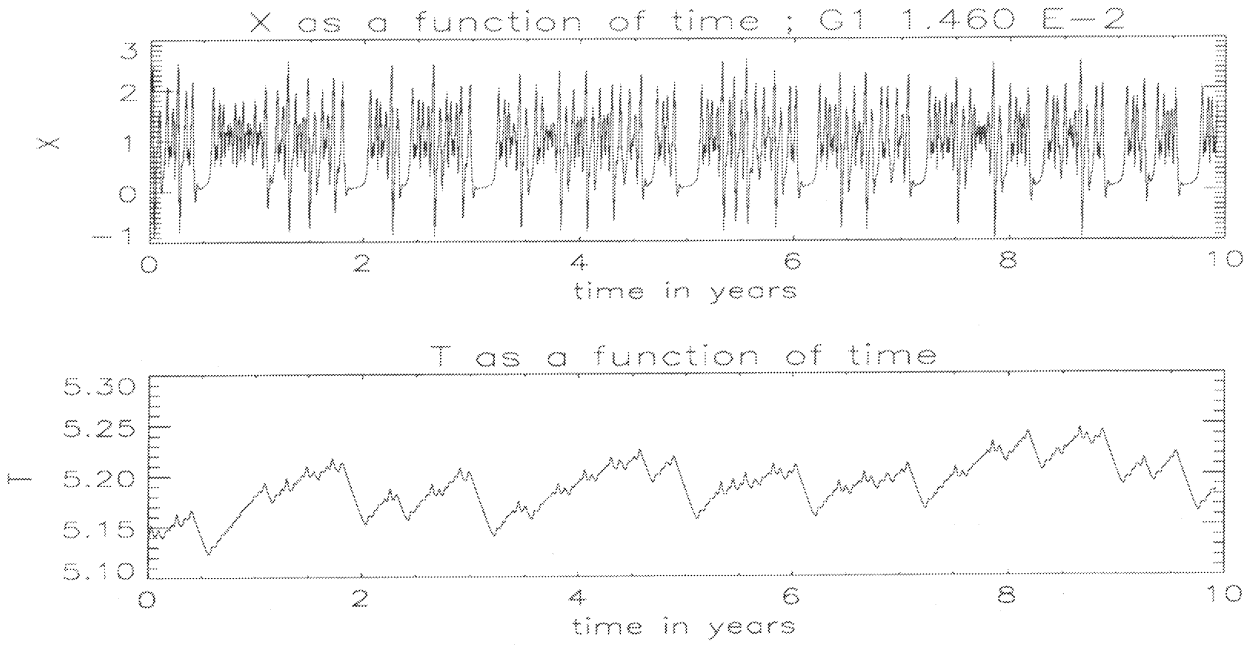

Figure 18: The intermittent signal, for $(F_1, G_1) = (1.2, 1.460) * 10^{-2}$.

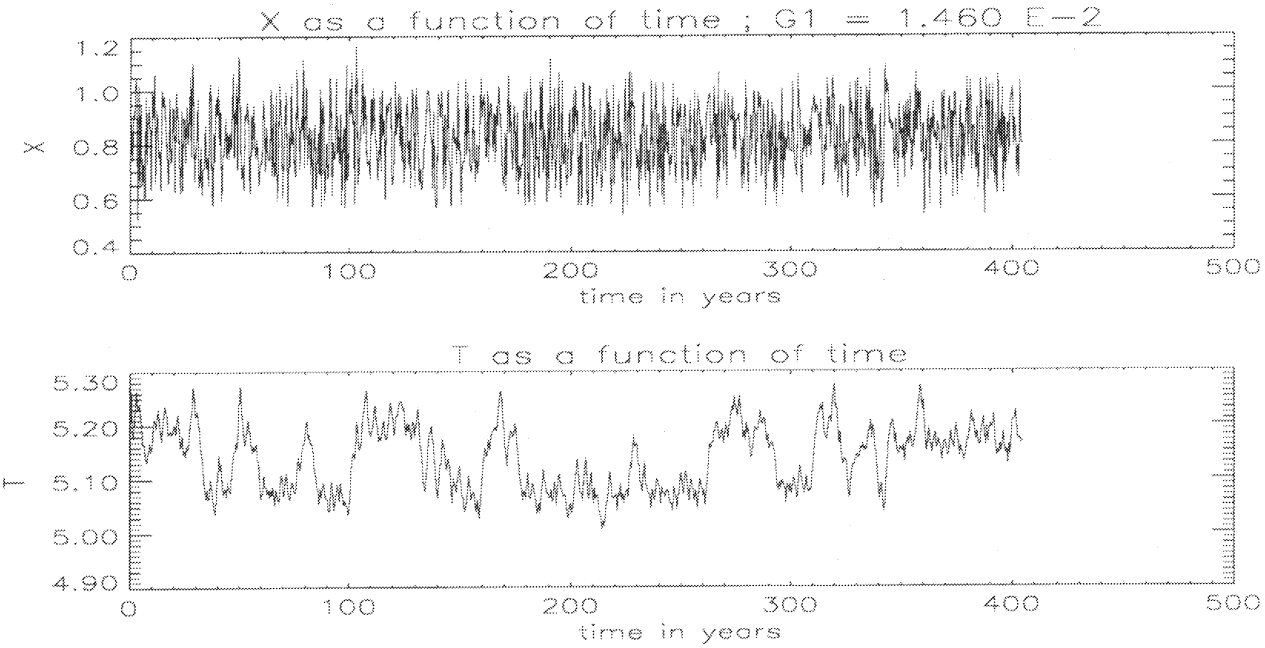

Figure 19: The averaged intermittent signal, for $(F_1, G_1) = (1.2, 1.460) * 10^{-2}$.

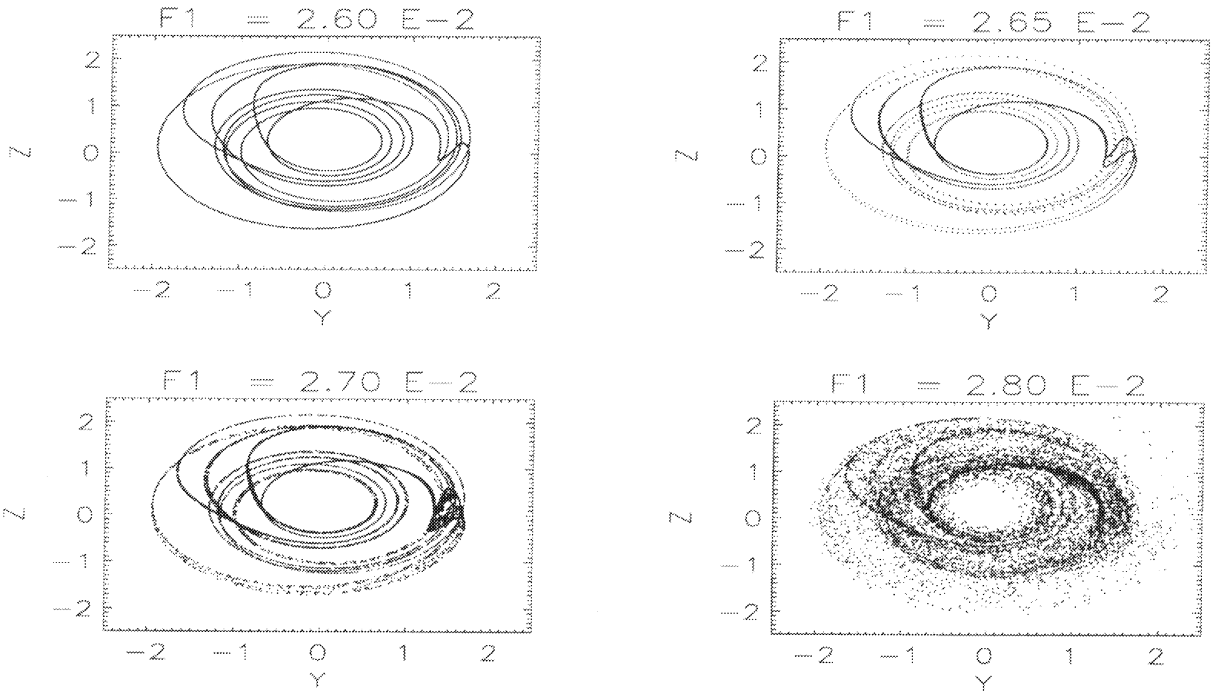

Figure 20: The system variables projected on the (Y, Z)-plane for various values of F_1 ; $(G_1 = 1.0 * 10^{-2})$

4.4.3 The transition from periodic to chaotic behaviour

We now come to the discussion of the last type of regime transition that has been found. The transition will be illustrated by the case in which the system changed from periodic to chaotic behaviour by increasing the parameter F_1. This process proves to be subtle in the sense that the chaotic behaviour close in (F_1, G_1)-space to the periodic regime closely resembles the periodic behaviour. The transition from periodic behaviour to chaotic behaviour takes place probably via period doubling bifurcations. In the projections in figure 20 we see successively : period doubling, below that the transition to chaos (noisy periodicity) and finally, fully developed chaos. The respective F_1-values are above the projections. At $F_1 = 2.60 * 10^{-2}$ we start off from an already quite intricate limit-cycle. For $F_1 = 2.65 * 10^{-2}$ the cycle has undergone a period doubling bifurcation : the limit-cycle appears to have "split" (the period has doubled). The chaotical behaviour sets in somewhat before $F_1 = 2.70 * 10^{-2}$, and seems to be constrained by an area in phase space that is close to the previous limit-cycle. In this noisy periodic behaviour the first (positive) Lyapunov exponent is very small $(L_1 = 0.022)$. As one would expect since the behaviour and power spectrum still closely resembles the periodic behaviour. For a plot of the power spectra for $F_1 = 2.65 * 10^{-2}$ and $F_1 = 2.70 * 10^{-2}$, see

figure 21. The Kaplan-Yorke dimension has the small value of 4.03. Also for the

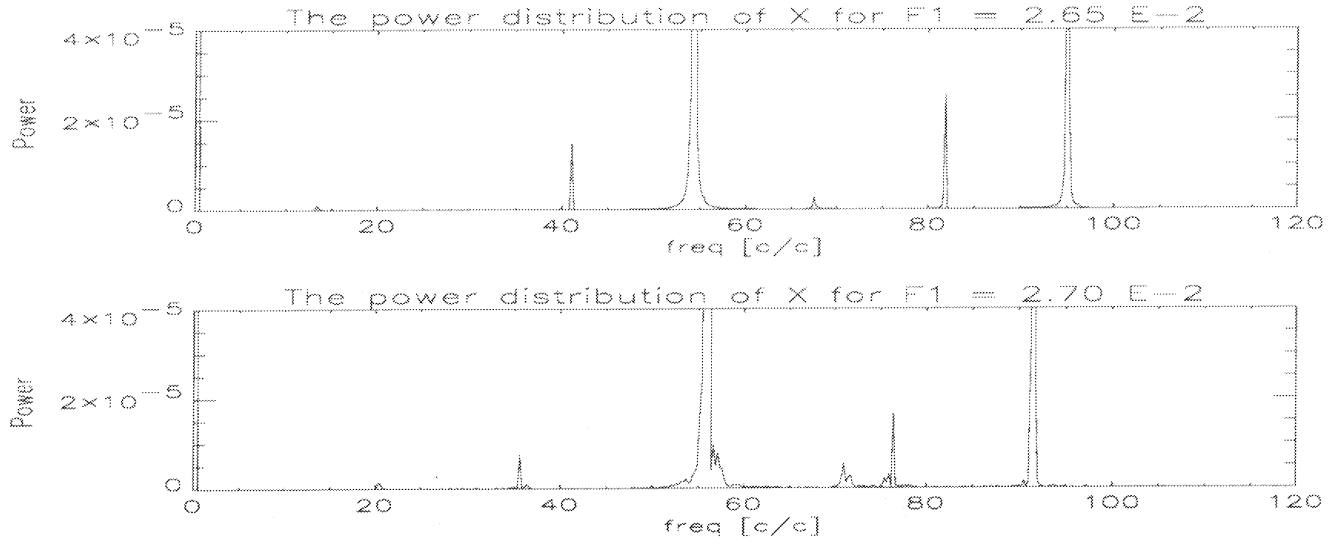

Figure 21: The power spectra for periodic behaviour : $F_1 = 2.65 * 10^{-2}$ and for noisy periodic behaviour : $F_1 = 2.70 * 10^{-2}$ ($G_1 = 1.0 * 10^{-2}$).

other areas in (F_1, G_1)-space we found that close to the regime transition there is a remarkable drop in the first Lyapunov exponent. The power spectrum also indicates the limited variance in the atmospheric signal. For $F_1 = 2.80 * 10^{-2}$ the system is fully chaotic again, displaying a wider range of possible frequencies. Also the plot in YZ-plane shows that more freedom is allowed. For the first Lyapunov exponent and the Kaplan-Yorke dimension holds :$L_1 = 0.266; D_{KY} = 4.38$. Thus we can assume that the system has again reached the fully chaotic regime. Note that the same type of behaviour takes place when we make the transition by varying parameter G_1. Another remarkable feature of the system is the asymmetry between the transition behaviour in both directions. The transition behaviour from chaotic to periodic behaviour is markedly different from the behaviour from periodic to chaotic behaviour (in both cases either the parameter F_1 or G_1 was increased).

5 Conclusions

The experiments seem to indicate a scenario in which the ocean is usually passive and follows the atmosphere. This puppet-like behaviour of the ocean is responsible for the high value of the Kaplan-Yorke dimension, in terms of attractor dimension it acts as a copy of the atmosphere (the two variables higher the attractor dimension of the atmosphere by two). This behaviour mimics that of more complicated coupled atmosphere ocean models. A small change in the parameters or initial conditions can cause a drastic change in the atmosphere model's behaviour. The ocean, in its turn dependent on the atmosphere-forcing, can cause these small parameter changes through the feedback. One would thus expect the effect of feedback to be rather obvious. From the experiments however, it proved difficult to distinguish between the complex behaviour and sensitive parameter dependence of the atmosphere and the effects that are introduced by introducing the coupling. But when close to a bifurcation point, where the atmospheric behaviour is very sensitive to parameter changes, the ocean can play an important role.

Another notable feature of the oceanic response, is that its signal displays power in a frequency-range (1-5 cycles per century) that is not dominant in the atmospheric signal that's forcing the ocean. Thus one would expect an increase in this frequency range of the atmospheric signal when feedback is introduced. Since now the atmosphere is forced by a signal that varies on a specific (long) time-scale. This effect was not yet obvious in the experimental data. Also care should be taken when chosing the integration scheme. Although the ocean displays mainly behaviour on the long time-scale, one should take an integration scheme that is as accurate as that for the atmosphere (see section 4.4.1). Note that the atmospheric dependence on the integration scheme of the ocean, during intermittent behaviour, also forms evidence for the subtle effect of feedback.

It also showed that in the ocean model used, salinity is a variable which can be 'frozen' in time without noticably influencing the dynamics. This only for each parameter set separately, as soon as either of the feedback parameters F_1 and G_1 is changed then also does the mean salinity. And the mean salinity has an influence on the atmosphere model via the thermohaline flow effect on the ocean temperature anomaly. In one specific case the atmosphere was forced from a chaotic regime into a periodic regime by fixing the salinity difference at another mean ($0.123 * 10{-}2$ unit) than it would adopt naturally for the chosen parameter set ($0.130 * 10^{-2}$ unit). Concluding : coupling can be a crucial factor although not always immediately obvious, to determine its effect specific experiments need to be devised.

Another interesting aspect which is probably strongly linked to feedback effects is the following : On the intermittent transition from chaos to a stable equilibrium there were two basic regimes visible with a long duration/timescale, see figure 19. In one of those regimes the average of the strength of the westerly current was smaller than in the other, resulting from a difference in the frequency of the intermittent

intervals. This difference may be the result of feedback effects. Because as we have seen the feedback via the ocean does probably not cause a visible change in the atmospheric attractor-shape. But it may be that by constantly pushing the atmosphere, on a long (oceanic) timescale, otherwise seldomly reached regions in phase space are visited more frequently. In the above mentioned intermittent behaviour, the region around the stable stationary attractor.

There are still many experiments which could lead to a better understanding of the system.
A few suggestions :
New investigations :
- It would be useful to keep track of the eigenvalues of the coupled system when close to one of the bifurcations observed.
- Force the ocean model with white noise and then monitor its response.
One expects the ocean to act as a kind of low-pass filter.
- Histogram of an atmospheric variable : in the feedback/no feedback case.
To see if the effect of feedback can be observed during fully chaotic behaviour.
- Is it possible to classify the bifurcation type for the transition from periodic to chaotic behaviour (for example with a Poincare plot)?
- Another way to investigate the effect of the feedback is by calculating the correlation between the atmospheric and oceanic signal (statistical approach). And this for varying parameters F_1 and G_1.
- In the intermittent case, does the coupled system reach the stable attractor if we wait long enough? This does not seem to be the case when we look at the data : there seems to be a repelling factor that pushes the system away from this attractor.
New Models :
New investigations might also include new models out of which the system is constructed :
- A different, more active ocean model.
- A different, physically better justifiable atmosphere model (this however does not contribute to the field of interest sketched here).

References

[1] Anastassiades, L., 1995: Numerical studies on the Lorenz-84 atmosphere model, KNMI WR 95-05

[2] Lenderink, G., 1992: Sensitivity and internal variability of the thermohaline circulation, KNMI unofficial report

[3] Lorenz, E.N., 1984: Irregularity: a fundamental property of the atmosphere, Tellus, **36A**, 98-110

[4] Roebber, P.J., 1995: Climate variability in a low order coupled atmosphere model, Tellus, **47A**, 473-494

[5] Saltzman, B., 1989: Folded resonance and seasonal vacillation in a thermally forced baroclininic wave model, Atmósfera, **2**, 131-154

[6] Schuster, H.G., 1984: Deterministic chaos : an introduction, Weinheim : Physic- Verlag

[7] Stommel, H., 1961: Thermohaline convection with two stable regimes of flow, Tellus, **13**, 224-230

[8] Wolf, A., J.B. Swift, H.L. Swinney and J.A. Vastano, 1985: Determining Lyapunov exponents from a time series, Physica, **16D**, 285-317

KNMI-Publicaties, Technische & Wetenschappelijke Rapporten gepubliceerd sedert 1988

Een overzicht van alle publicaties van het Koninklijk Nederlands Meteorologisch Instituut die tussen 1849 en 1987 werden uitgegeven, wordt u op verzoek toegezonden door de Bibliotheek van het KNMI, postbus 201, 3730 AE De Bilt, tel. 030 - 2 206 855, fax. 030 - 2 210 407.

	KNMI-publicatie met nummer:	
150-27	Normalen en extreme waarden van 15 hoofdstations voor het tijdvak 1961-90 / samenst. H.J. Krijnen ...[et al.]	1992
165-5	Historische weerkundige waarnemingen: beschrijving antieke meetreeksen / H.A.M. Geurts en A.F.V. van Engelen	1992
172	Vliegen in weer en wind: geschiedenis van de luchtvaartmeteorologie / Tj. Langerveld	1988
173	Werkdocument verspreidingsmodellen / red. H. van Dop ; in samenwerking met het RIVM	1988
174	Ons klimaat, onze planeet / voorw. H. Tennekes ; inleiding C.J.E. Schuurmans ; met bijdr. van H. van Dop ...[et al.]	1989
175	Klimaat-onderzoek Westland ten behoeve van kustuitbreiding / W.H. Slob	1989
176	Stormenkalender: chronologisch overzicht van alle stormen langs de Nederlandse kust 1964-1990 / B. Augustijn, H. Daan ...[et al.]	1990
177	Description of the RIVM-KNMI PUFF dispersion model / G.H.L. Verver ...[et al.]	1990
178	Modules A & B / Bureau Vorming en Opleiding **[uitsluitend intern beschikbaar]**	1991
179	Catalogus van aardbevingen in Nederland / G. Hougast	1991
179a	Catalogus van aardbevingen in Nederland : 2e, gewijzigde druk / G. Houtgast	1992
180	List of acronyms in environmental sciences / [P. Geerders]	1991
180a	List of acronyms in environmental sciences : revised edition / [P. Geerders and M. Waterborg]	1995
181	Nationaal gebruik van de groepen 7wwW1W2 en 960ww voor landstations / [samenst. H. van Drongelen ea.]	1992
181a	FM12 Synop : internationale en nationale regelgeving voor het coderen van de groepen 7wwW1W2 en 960ww	1995
182	Wijziging aeronautische codes : 1 juli 1993 / [P.Y. de Vries en A.A. Brouwer]	1993
183-1	Rainfall in New Guinea (Irian Jaya) / T.B. Ridder	1995
183-2	Vergelijking van zware regens te Hollandia (Nieuw Guinea), thans Jayapura (Irian Jaya) met zware regens te De Bilt / T.B. Ridder	1995
183-3	Verdamping in Nieuw-Guinea, vergelijking van gemeten hoeveelheden met berekende hoeveelheden / T.B. Ridder	1995
183-4	Beschrijving van het klimaat te Merauke, Nieuw Guinea (Irian Jaya) in verband met de eventuele vestiging van een zoutwinningsbedrijf aldaar / T.B. Ridder en H.W.H. Weeda	1995
183-5	Overzicht van klimatologische en geofysische publikaties betreffende Nieuw-Guinea / T.B. Ridder	1995
184	Inleiding tot de algemene meteorologie : studie-uitgave / B. Zwart, A. Steenhuisen, m.m.v. H.J. Krijnen	1994
184a	Inleiding tot de algemene meteorologie : studie uitgave ; 2e, geheel herziene druk / B. Zwart, A. Steenhuisen, m.m.v. H.J. Krijnen ea.	1995
185	Handleiding voor het gebruik van sectie 2 van de FM 13-X SHIP code door stations op zee / KNMI; Kon. Luchtmacht; Kon. Marine	1994
185a	Handleiding voor het gebruik van sectie 2 van de FM 13-X SHIP-code voor waarnemers op zee / KNMI; Kon.Luchtmacht, Kon.Marine	1995
(-)	Zonnestraling in Nederland / C.A. Velds (i.s.m. uitgeverij Thieme in de serie Het klimaat van Nederland; 3)	1992

	Technisch rapport = technical report (TR) - ISSN 0169-1708	
103a	Wind-chill [geheel herziene versie] / B. Zwart	1992
105	Description of the Cabauw turbulence dataset 1977-1979 / C. Hofman	1988
106	Automatische detektie van inversies met sodar / A.C.M. Beljaars en R. Agterberg	1988
107	Numerieke atmosfeermodellen / A.P.M. Baede	1988
108	Inpassing van Meteosat informatie in de meteorologische besluitvorming / J. Roodenburg	1988
109	Opmeting van het aardmagneetveld in Nederland, herleid naar 1985 / J.H. Rietman	1988
111	Van Penman naar Makkink: een nieuwe berekeningswijze voor de klimatologische verdampingsgetallen / red. J.C. Hooghart ...[et al.]	1988
112	Description of a software library for the calculation of surface fluxes / A.C.M. Beljaars ...[et al.]	1989
113	Menghoogteberekeningen voor het Europees continent: een vergelijkend onderzoek / M.P. Scheele en H. van Dop	1989
114	Operational WAMS statistics over the period December 1986 - March 1987 / R.A. van Moerkerken ...[et al.]	1989
115	Mesoscale terrain roughness mapping of the Netherlands / R. Agterberg and J. Wieringa	1989
116	Geschiedenis van de landbouwmeteorologie in Nederland tot 1972 / J.P.M. Woudenberg	1989
117	Instabiliteiten rond de straalstroom / R.P. Henzen	1989
118	Verfificatie van de GONO golfverwachting over de periode oktober 1987 - april 1988 / R.A. van Moerkerken	1989
119	Spectra en gradienten van hoge windsnelheden te Cabauw tot 200 meter / R.W.M. Meijer	1989
120	About the possibilities of using an air transformation model in Tayun, Shanxi province, China / J. Reiff ...[et al.]	1989
121	The effect of wave data assimilation of the numerical simulation of wave energy advection / M. de las Heras ...[et al.]	1990
122	Objective analysis of precipitation observations during the Chernobyl episode / M.P. Scheele and G.H. Verver	1990
123	The use of satellite data in the ECMWF analysis system / K. Lablancz	1990
124	A primitive equation model for the Equatorial Pacific / M.A.F. Allaart and A. Kattenberg	1990
125	Technical description of the high-resolution air mass transformation model at KNMI / E.I.F. de Bruin ...[et al.]	1990
126	Verificatie kwantitatieve neerslagverwachting korte termijn (proefperiode) voor 5 regio's / D. Messerschmidt	1990
127	Quantitative processing of Meteosat-data: implementation at KNMI: applications / S.H. Muller	1990
128	A primary experiment of statistical interpolation schemes used in sea wave data assimilation / Gao Quanduo	1990
129	Coordinate conversions for presenting and compositing weather radar data / H.R.A. Wessels	1990
130	Flux-profile relationships in the nocturnal boundary layer / P. Bouwman	1990
131	The implementation of the WAQUA/CSM-16 model for real time storm surge forecasting / J.W. de Vries	1991
132	De luchttemperatuur boven West-Ameland / F. Ynsen	1991
133	Seizoenverloop en trend in de chemische samenstelling van de neerslag te Lelystad / T.A. Buishand en J.H. Baard	1991
134	Technical description of LAM and OI: Limited Area Model and Optimum Interpolation analysis / W.C. de Rooy ...[et al.]	1991
134a	Technical description of LAM and OI: Limited Area Model and Optimum Interpolation analysis, 2nd edition / W.C. de Rooy ...[et al.]	1992
135	Relatieve trajectorien in en rond een depressie / J.P.A.J. van Beeck	1991
136	Bepaling van een directe en diffuse straling en van zonneschijnduur uit 10-minuutwaarden van de globale straling / W.H. Slob ...[et al.]	1991
137	LAM en NEDWAM statistics over the period October 1990 - April 1991 / R.A. van Moerkerken	1991
138	Dagsom van de globale straling : een rekenmethode en verwachtingsverificatie / M.C. Nolet	1991
139	A real-time wave data quality control algorithm / Maria Paula Etala	1991
140	Syllabus Fysische Meteorologie I / H.R.A. Wessels	1991
141	Systeembeschrijving Mist Voorspel Systeem MIVOS / D. Blaauboer, H.R.A. Wessels en S. Kruizinga	1992
142	Het nachtelijk windmaximum : een interactieve verwachtingsmethode / N. Maat en H. Bakker	1992

143	Neerslagverificatie LAM / W.C. de Rooy en C. Engeldal	1992
144	Aanpassing vocht-bedekkingsgraadrelaties in het LAM / W.C. de Rooy	1992
145	Een verificatie van de Eurogids, de gidsverwachting voor vervoer en toerisme / H.G. Theihzen	1992
146	The earth radiation budget experiment : overview of data-processing and error sources / Arnout J. Feijt	1992
147	On the construction of a regional atmospheric climate model / Jens H. Christensen and Erik van Meijgaard	1992
148	Analyse van torenwindgegevens over het tijdvak 1977 tot en met 1991 / Gertie Geertsema	1992
149	The performance of drag relations in the WAQUA storm surge model / J.R.N. Onvlee	1993
150	Verifications of 31 retrievals vis-à-vis radiosonde observations / G.J. Prangsma	1993
151	Het Synoptisch Symposium : een verslag / red. H.G. Theihzen	1993
152	The ACIFORN hydrological programme : the water cycle of a Douglas fir forest / F.C. Bosveld ...[et al.]	1993
153	Het APL+-prgramma / R.M. van Westrhenen	1993
154	The effect of spatial averaing on threshold exceedances of daily precipitation amounts / T.A. Buishand,	1993
155	Neerslagvergelijking van Espelo ten opzichte van het omgevingsgemiddelde / J.P.M. van Dun en J. Verloop	1993
156	On the effects of limited spectral resolution in third-generation wave models / I.V. Lavrenov and J.R.A. Onvlee	1993
157	Meteorologische evaluatie van de zichtmetingen langs de A16 / H.R.A. Wessels	1993
158	Het programma voor berekening van zonneschijnduur uit globale straling / U. Bergman	1993
159	Verificatie weersverwachtingen 1955 - 1993 / H. Daan	1993
160	Drie objectieve indices voor clear-air turbulence nader bekeken / H. Bakker	1993
161	The ASGASEX experiment / W.A. Oost	1994
162	TEBEX observations of clouds and radiation -potential and limitations / P. Stammes ...[et al.]	1994
163	Evaluatie kwaliteitsonderzoek mistdata "Mistprojekt A-16" Breda / M. van Berchum	1994
164	Standaard stralingsmetingen met een zonnevolger / A.C.A.P. van Lammeren en A. Hulshof	1994
165	Neurale netwerken versus lineaire regressie / R.M. Meuleman	1994
166	Seismische analyse van de aardbeving bij Alkmaar op 6 augustus 1994 / [SO]	1994
167	Seismische analyse van de aardbeving bij Alkmaar op 21 september 1994 / [SO]	1994
168	Analyse van het seismische risico in Noord-Nederland / Th. de Crook, B. Dost en H.W. Haak	1995
169	Evaluatie van neerslagprognoses van numerieke modellen voor de Belgische Ardennen in december 1993 / Erik van Meijgaard	1994
170	DARR-94 / C.P.G. Lomme	1994
171	EFEDA-91 : documentation of measurements obtained by KNMI / W.A.A. Monna ...[et al.]	1994
172	Cloud lidar research at the Royal Netherlands Meteorological Institute and KNMI2B2 version 2 cloud lidar analysis software documentation / Alexandre Y. Fong and André C.A.P. van Lammeren	1994
173	Measurements of the structure parameter of vertical wind-velocity in the atmospheric boundary layer / R. van der Ploeg	1995
174	Report of the ASGASEX'94 workshop / ed. by W.A. Oost	1995
175	Over slecht zicht, bewolking, windstoten en gladheid / J. Terpstra	1995
176	Verification of the WAQUA/CSM-16 model for the winters 1992-93 and 1993-94 / J.W. de Vries	1995
177	Nauwkeuriger nettostraling meten / M.K. van der Molen en W. Kohsiek	1995
178	Neerslag in het stroomgebied van de Maas in januari 1995: waarnemingen en verificatie van modelprognoses / Rudmer Jilderda ...[et al.]	1995
179	First field experience with 600PA phased array sodar / Henk Klein Baltink	1995
180	Een Kalman-correctieschema voor de wegdektemperatuurverwachtingen van het VAISALA-model / A. Jacobs	1995
181	Calibration study of the K-Gill propeller vane / Marcel Bottema	1995
182	Ontwikkeling van een spectraal UV-meetinstrument / Frank Helderman	1995
183	Rainfall generator for the Rhine catchment : a feasibility study / T. Adri Buishand and Theo Brandsma	1996
184	Parametrisatie van mooi-weer cumulus / M.C. van Zanten	1995
185	Interim report on the KNMI contributions to the second phase of the AERO-project / Wiel Wauben, Paul Fortuin ...[et al.]	1995
186	Seismische analyse van de aardbevingen bij Middelstum (30 juli 1994) en Annen (16 augustus 1994 en 31 januari 1995) / [SO]	1995
187	Analyse wenselijkheid overname RIVM-windmeetlokaties door KNMI / H. Benschop	1996
188	Windsnelheidsmetingen op zeestations en kuststations: herleiding waarden windsnelheden naar 10-meter niveau / H. Benschop	1996
189	On the KNMI calibration of net radiometers / W. Kohsiek	1996
190	NEDWAM statistics over the period October 1994 - April 1995 / F.B. Koek	1996
191	Description and verification of the HIRLAM trajectory model / E.I.F. de Bruijn	1996
192	Tiltmeting : een alternatief voor waterpassing ? / H.W. Haak	1996

Wetenschappelijk rapport = scientific report (WR) - ISSN 0169-1651

88-01	Central Sudan surface wind data and climate characteristics / E.H. ABu Bakr
88-02	Startocumulus modeling / P.G. Duynkerke
88-03	Naar een niet-linear wateropzetmodel : stand van zaken februari 1988 / C.J. Kok
88-04	The boundary layer wind regime of a representative tropical African region, central Sudan / E.H. ABu Bakr
88-05	Radiative cooling in the nocturnal boundary layer / S.A. Tjemkes
88-06	Surface flux parameterization schemes : developments and experiences at KNMI / A.A.M. Holtslag and A.C.M. Beljaars
89-01	Instability mechanisms in a barotropic atmsophere / R.J. Haarsma
89-02	Climatological data for the North Sea based on observations by volutary observing ships over the period 1961-1980 / C.G. Korevaar
89-03	Verificatie van GONO golfverwachtingen en van Engelse fine-mesh winden over de periode oktober 1986 - april 1987 / R.A. van Moerkerken
89-04	Diagnostics derivation of boundary layer parameters from the outputs of atmospheric models / A.A.M. Holtslag ...[et al.]
89-05	Statistical forecasts of sushine duration / Li Zhihong and S. Kruizinga
90-01	The effect of a doubling atmospheric CO2 on the stormtracks in the climate of a GCM / P.C. Siegmund
90-02	Analysis of regional differences of forecasts with the multi-layer AMT-model in the Netherlands / E.I.F. de Bruin, Li Tao Guang ...[et al.]
90-03	Description of the CRAU- data-set: Meteosat data, radiosonde data, sea surface temperatures : comparison of Meteosat and Heimann-data / S.H. Muller, H. The, W. Kohsiek and W.A.A. Monna
90-04	A guide to the NEDWAM wave model / G. Burgers
91-01	A parametrization of the convective atmospheric boundary layer and its application into a global climate model / A.A.M. Holtslag ...[et al.]
91-02	Turbulent exchange coefficients over a Douglas fir forest / F.C. Bosveld
92-01	Experimental evaluation of an arrival time difference lightning positioning system / H.R.A. Wessels
92-02	GCM control run of UK Met.Office compared with the real climate in the Northwest European winter / J.J. Beersma
92-03	The parameterization of vertical turbulent mixing processes in a General Circulation Model of the Tropical Pacific / G. Janssen
92-04	A scintilation experiment over a forest / W. Kohsiek
92-05	Grondtemperaturen / P.C.T. van der Hoeven en W.N. Lablans
92-06	Automatic supression of anomalous propagation clutter for noncoherent weather radars / H.R.A. Wessels ...[et al.]

93-01 Searching for stationary stable solutions of Euler's equation / R. Salden
93-02 Modelling daily precipitation as a function of temperature for climatic change impact studies / A.M.G. Klein Tank and T.A. Buishand
93-03 An analytical conceptual model of extratropical cyclones / L.C. Heijboer
93-04 A synoptic climatology of convective weather in the Netherlands / Dong Hongnian
93-05 Conceptual models of severe convective weather in the Netherlands / Dong Hongnian
94-01 Seismische analyse van aardbevingen in Noord-Nederland : bijdrage aan het multidisciplinaire onderzoek naar de relatie tussen gaswinning en aardbevingen / H.W. Haak en Th. de Crook
94-02 Storm activity over the North Sea and the Netherlands in two climate models compared with observations / J.J. Beersma
94-03 Atmospheric effects of high-flying subsonic aircraft / W. Fransen
94-04 Cloud-radiation-hydrological interactions : measuring and modeling / A. Feijt ...[et al.]
94-05 Spectral ultraviolet radiation measurements and correlation with atmospheric parameters / F. Kuik and H. Kelder
95-01 Transformation of precipitation time series for climate change impact studies / A.M.G. Klein Tank and T.A. Buishand
95-02 Internal variability of the ocean generated by a stochastic forcing / M.H.B. van Noordenburg
95-03 Applicability of weakly nonlinear theory for the planetary-scale flow / E.A. Kartashova
95-04 Changes in tropospheric NOx and O3 due to subsonic aircraft emissions / W.M.F. Wauben ...[et al.]
95-05 Numerical studies on the Lorenz-84 atmosphere model / Leonardo Anastassiades
95-06 Regionalisation of meteorological parameters / W.C. de Rooy
95-07 Validation of the surface parametrization of HIRLAM using surface-based measurements and remote sensing data / A.F. Moene, H.A.R. de Bruin ...[et al.]
95-08 Probabilities of climatic change : a pilot study / Wieger Fransen (ed.) and Alice Reuvekamp